Tikrit Journal of Engineering Sciences

IRAQI Academic Scientific Journals | TJES Tikrit Journal of Engineering Sciences

Article | Tikrit Journal of Engineering Sciences (2026); 33 (1): 2349

Open Access

Enhancing High-Density Polyethylene with Yellow Oil Fly Ash: Mechanical, Physical, and Tribological Behavior Analysis

Saif S. Irhayyim [1*], Farouk M. Mahdi [1], Saad R. Ahmed [1], Sanjeev Khanna [2], Mohammed Mutanbak [3]

[1] Mechanical Department, College of Engineering, Tikrit University, Tikrit, Iraq.
[2] Mechanical and Aerospace Engineering Department, College of Engineering, University of Missouri Columbia, Columbia, USA.
[3] Civil and Architectural Engineering Department, College of Engineering and Computer Science, Jazan University, Jazan, Saudi Arabia.

Emails:
Saif S. Irhayyim | Farouk M. Mahdi | Saad R. Ahmed | Sanjeev Khanna | Mohammed Mutanbak

Abstract:

Fly ash-reinforced polymer composites, known for their advantageous properties and environmental sustainability, have gained popularity. Heavy fuel oil fly ash, particularly yellow oil fly ash (YOFA), could serve as an enforcement component due to its mechanical properties. This study aims to introduce YOFA, a novel type of heavy fuel oil fly ash, as a potential reinforcement in high-density polyethylene (HDPE). The HDPE/YOFA composites were prepared using the injection molding technique after the extrusion blending process. The effect of YOFA content and particle size on mechanical and physical properties was investigated. The results revealed that the hardness slightly declined when the YOFA content and particle size were increased compared with the net HDPE. In contrast, the experimental density showed a positive correlation with the YOFA content and a negative correlation with the YOFA particle size. Additionally, the void content, water absorption, and thickness swelling increased gradually with YOFA content and particle size. A dry sliding wear test was conducted using the pin-on-disc method, and the following factors were chosen as independent variables: YOFA content, particle size of YOFA, applied load, and sliding time during the wear test. This method significantly affects two responses: wear loss and wear rate. Under steady-state conditions, wear resistance decreases with YOFA particle size and normal applied load. It also decreases with YOFA content up to 2 wt.%, followed by a gradual improvement up to 8 wt.%. On the other hand, with increasing sliding time, wear loss considerably increases while the wear rate significantly improves. The wear test conditions have been optimized using a full factorial design and Taguchi approach. A total of 320 experimental runs, each with one replication, have been conducted. The ANOVA analysis confirmed the robustness of the designed experiment, revealing that the factors contributing significantly, in order of importance, were sliding time, applied load, particle size of YOFA, and YOFA content. To minimize wear loss, the ideal settings were 8 wt.% YOFA content, the smallest particle size, an applied load of 5 N, and a sliding time of 5 minutes. Conversely, for optimizing the wear rate, the parameters were identical except for a longer sliding time of 20 minutes.

Keywords:

HDPE; Oil fly ash; Physical properties; Dry sliding wear; Full factorial design; Taguchi approach.

Highlights:

- Improved environmental sustainability by using industrial waste in composites.
- HDPE is reinforced with a novel type of fly ash called yellow oil fly ash.
- Hardness decreased slightly with increasing YOFA content and particle size.
- Wear resistance improved significantly with increasing YOFA content.

Corresponding Author*:

Saif S. Irhayyim
Mechanical Department, College of Engineering, Tikrit University, Tikrit, Iraq.

Article History:

Received:	30	Jul.	2024
Received in revised form:	06	Sep.	2024
Accepted:	05	Jan.	2025
Final Proofreading:	15	Mar.	2026
Available online:	03	Jun.	2026

Citation:

Irhayyim SS, Mahdi FM, Ahmed SR, Khanna S, Mutanbak M. **Enhancing High-Density Polyethylene with Yellow Oil Fly Ash: Mechanical, Physical, and Tribological Behavior Analysis**. *Tikrit Journal of Engineering Sciences* 2026; **33**(1): 2349.

https://doi.org/10.25130/tjes.33.1.14

1.INTRODUCTION

Fly ash (FA) is a synthetic material produced as a byproduct in various heavy industries, including petroleum, cement, and coal-fired power plants. Coal-powered power plants produce a significant amount of FA, which is the coal combustion residue. When coal is completely burned, the components of coal, mainly the oxides of silica and alumina, convert into FA. Around 80% of FA is entrapped during combustion in bag filters, electrostatic precipitators, and flue gases [1]. The significant production of FA can have adverse environmental effects, including its contribution to global climate change. Improper disposal of FA can lead to environmental contamination, with high concentrations of phytotoxic heavy metals harmful to fish and aquatic organisms [1,2]. The leaching of heavy metals from coal FA ponds can cause phytotoxicity, soil and vegetation contamination, and water pollution of ground and surface water [1]. Fossil ash (FA) can be integrated into materials to mitigate environmental impacts and reduce costly disposal procedures, resulting in the development of affordable, high-value products. Researchers have demonstrated that incorporating FA significantly enhances the strength of construction materials, particularly in combination with thermoplastic polymers to form robust composites. Further studies indicate that modifying FA can enhance its compatibility with diverse polymers, paving the way for advanced polymer composites with potential applications across the construction and automotive sectors [3, 4]. While many innovative strategies are published in academic periodicals, one critical real-world issue that has been overlooked is the recyclability of composite materials. Thermoplastic polymer composites, for example, have limited lifetimes, and currently, almost 95% of such composites end up in landfills [5]. It is essential to focus on the use of non-ecofriendly FA in the development of polymer composites. Additionally, recycling and reusing these composites is crucial. It is also necessary to investigate the compositional parameters of the composites, including filler size, filler concentration, and the compatibility between the filler and the matrix [1]. Polymer matrix composites (PMCs) are highly stable and possess superior physical properties due to the incorporation of reinforcing fibers, particles, or fabrics. Adding fillers can provide good mechanical and tribological properties, but it can also cause some mechanical properties to be lost due to their incompatibility with the polymer matrix. Thermoplastic polymers are widely used in various applications, including home appliances, the military, sports, aerospace, biomedical, and automotive industries. These polymers are widely used in the production of polymer composites due to their unique properties, including lightweight, wear resistance, corrosion resistance, vibration-free operation, high strength, and more. They are typically used to fabricate components for the automotive industry, such as dashboards, doors, gears, bearings, brake pads, clutches, and bushes [5–8]. Among the various matrix materials, petroleum-derived thermoplastics are considered the best choice [9, 10]. Various thermoplastics can be used, such as polypropylene (PP), polyamides (PA), and polyethylene (PE). Among these, high-density polyethylene (HDPE) is particularly stable and is commonly used in various applications. These applications include automotive components, building materials, consumable packaging, and electronics. HDPE is a type of plastic that has a semi-crystalline structure. It is mechanically strong and exhibits resistance to moisture and chemical compounds. These characteristics make it highly beneficial in preventing the environmental degradation of the polymer and the release of microplastics [7, 9, 11, 12]. Tribology is a branch of materials science that deals with the study of surfaces in motion, focusing on friction, lubrication, and wear. The friction and wear resistance of plastic composites is crucial when they come in contact with other moving materials. When composites wear out, it can lead to significant problems in various industries and applications, reducing their durability and efficiency. The primary causes of wear in polymer composites are adhesion and deformation; however, adhesion is primarily responsible for most of the friction. Adhesion occurs when weak bonding forces between the polymer chains of the material break. Multiple factors, including additives, fibers, tribological environment, and composite geometry, influence the wear resistance of polymers [13, 14]. Recent studies have investigated the effects of incorporating FA particles into PE matrix composites, with a specific focus on their mechanical properties. Several studies have investigated the impact of adding FA on the wear resistance and mechanical properties of PE. Chand et al. [10] investigated the abrasive wear behavior of LDPE reinforced with untreated and silane-treated cenosphere FA. It was concluded that chemical treatment with silane can significantly enhance the abrasion resistance of cenosphere-filled FA LDPE. Treating FA with organosilane enhances the mechanical properties of LDPE composites. As the applied load and sliding duration remain constant, the wear rate increases with the increase in speed. However, the wear rate of the LDPE composite increased as the weight content of FA increased, probably

due to increased filler-filler interaction. The optimal concentration for improved mechanical and tribological performance was achieved at 10 wt.% cenosphere FA. Sheykh et al. [13] comparatively investigated the effect of rice husk ashes, bagasse, and nano-SiO_2 on the friction coefficient and wear resistance of HDPE/lignocellulosic fiber composites. Adding both ashes and silica nanoparticles improved the wear resistance of the composites; however, this improvement came at the cost of negatively impacting water absorption and thickness swelling. Rice husk ash with a higher SiO_2 content was found to have a more significant positive impact on wear resistance than bagasse ash. However, using ashes led to a significant decrease in other mechanical strengths of the composites, such as Izod impact resistance, modulus of elasticity, and modulus of rupture. Adding 5% less ash to the plastic composites is recommended to prevent a significant reduction of other mechanical properties. In general, nano-silica has proven more effective than rice husk and bagasse ashes in improving wear resistance. Alshabander et al. [15] studied the mechanical properties and thermal conductivity of coal FA/recycled HDPE (RHDPE) composites. It was observed that coal FA/RHDPE composites were stronger and stiffer than RHDPE. However, the impact strength of the composites decreased with an increase in the filler concentration. This behavior is due to the reduction of the material's elasticity caused by adding filler. As a result, the matrix's deformability decreases, losing its ability to absorb deformation energy. The wear rate is lower in the coal FA/RHDPE composite than in the unfilled recycled polymer. Besides, it has been observed that the thermal conductivity of the coal FA/RHDPE composite increases with an increase in filler content. Previous studies about this investigation have predominantly focused on using coal and black oil FA to reinforce HDPE. Besides, they neglect to study the properties of HDPE reinforced with a novel type of FA, called yellow-oil FA (YOFA) particles, which are derived as a byproduct from the power stations that utilize heavy fuel oil treated with magnesium oxide (MgO). The novelty of the present study lies in bridging this knowledge gap by thoroughly examining HDPE-YOFA composites, which have been previously unstudied. This study will facilitate their potential utilization in critical components within the construction, aerospace, and automobile industries. Furthermore, this research endeavor aims to deliver a qualitative and quantitative analysis of the physical, hardness, and tribological characteristics under typical operational conditions. By expanding the scope of the investigation beyond conventional coal and black oil FA, this study introduces a novel approach to reinforcing HDPE composites, thereby significantly contributing to the existing body of knowledge.

2.MATERIALS AND METHODS

2.1.Materials

2.1.1.Matrix Material

Petroleum-based thermoplastic high-density polyethylene (HDPE) (Grade: SABIC HDPE B5429) was purchased from Saudi Basic Industries Corporation (SABIC), Saudi Arabia. HDPE granules have a melt flow rate (MFR) of 29 g/10 min at 190 °C/21.6 kg (ASTM D1238), a density of 0.954 g/cm^3 at 23 °C (ASTM D1505), Vicat softening temperature of 124 °C (ASTM D1525), a brittleness temperature of <-75 °C (ASTM D746), and tensile strength at yield of 28 MPa (ASTM D638).

2.1.2.Reinforcement Material

YOFA samples were collected from the Al-Qayyarah power station in Nineveh, Iraq. This power station used heavy fuel oil treated with MgO to prevent corrosion in turbine blades. The MgO reacts with vanadium in the fuel oil to mitigate corrosion and maintain the operational integrity of the turbines. Magnesium can be added to heavy fuel oil in different forms. It can be small, dispersed particles, such as oxide or carbonate, or dissolved in oil (naphthalene or acetate). Magnesium can also be added to an aqueous solution, such as sulfates or chlorides. Magnesium oxide additives are essential for prolonging the lifespan of steel components, such as boiler tubes and turbine blades, which use gaseous fuels (residual fuel). This behavior occurs because magnesium oxide can form a stable vanadate ($Mg_3V_2O_8$), as shown in Eq. (1), which remains solid at the working temperatures in steam boiler tubes and gas turbine blades [16, 17].

$$3MgO + V_2O_5 \rightarrow Mg_3V_2O_8 \quad (1)$$

The compound ($Mg_3V_2O_8$) is independent of the amount of (MgO) when the ratio of (MgO: V_2O_5) is below (1:3). In such cases, the reaction products contain ($MgO_3V_2O_5$). However, an excess in (V_2O_5) occurs when the ratio is below (1:3). Conversely, an excess in (V_2O_5) and (MgO) occurs when the ratio exceeds (1:3). The compound (V_2O_5: MgO) is affected by the presence of (SO_3/SO_2) in the air, which arises from sulfur pollutants [17, 18]. The following chemical equation can represent this:

$$SO_2 + \frac{1}{2}O_2 \rightarrow SO_3 \quad (2)$$

When there is a sufficient amount of SO_3 present, MgO reacts with sulfur and forms a compound called $MgSO_4$:

$$MgO + SO_3 \rightarrow MgSO_4 \quad (3)$$

The compound $MgSO_4$ can react with V_2O_5 to form sulfites and $2MgO.V_2O_5$ fused to boiler tubes and turbine blades [17, 19]:

$$MgSO_4 + V_2O_5 \rightarrow 2MgO.V_2O_5 + SO_3 \quad (4)$$

YOFA samples were collected directly from the areas where heavy fuel is burned to produce electricity. They were gathered from the

station's mechanical hoppers as coarse particles and used without chemical or physical treatment. These samples were then combined and homogenized through appropriate coning and quartering techniques. Approximately 3 kg of YOFA was collected on different occasions, and all the samples were mixed to create a final mixture for conducting extraction experiments. The YOFA is yellow and has a density of 2.18 g/cm³. Its morphological properties were evaluated using scanning electron microscopy (SEM) and energy-dispersive X-ray spectrometry (EDX), which produced high-magnification images. The amount of organic material in a YOFA sample, known as the total organic content (TOC), was determined using ELTRACW multiphase CO_2/H_2O determination. The YOFA's chemical composition, as shown in Table 1, was analyzed using a Shimadzu XRF-1800 Sequential X-Ray Fluorescence Spectrometer from Japan, which uses X-ray fluorescence analysis measurements. The FA produced in this study contains very low levels of Al_2O_3 and Fe_2O_3 compared to FA produced by burning coal or oil shale. The standard chemical requirements for ASTM C618 [20] state that the sum of SiO_2, Al_2O_3, and Fe_2O_3 content must be 70% for class F and 50% for class C. The total organic content of the FA produced in this study is 7.46 wt.%. In a study by Bayat [21], the Al_2O_3 + SiO_2 contents for Turkish coal FA were higher than 65 wt.% for all samples, and the loss on ignition (LOI) ranged from 1.33 to 6.47 wt.% for the 7 types of coal FA samples investigated. In this study, the LOI is 8.27%. In comparison, Ghouti et al. [22, 23] studied the properties and characterization of FA produced from heavy fuel oil treated with MgO. The FA was collected from the Al-Aqaba thermal power station in southern Amman, Jordan. The study found that the total organic content in the FA is 30.88%, and the LOI is 37.23%. Additionally, the FA contains 13.12% of MgO and 3% of vanadium.

Table 1 Chemical Composition of YOFA Particles.

Oxide composition		Elemental composition	
Component	**wt. %**	**Component**	**ppm**
Al2O3	0.095	S	302461
Fe2O3	2.869	Co	588
CaO	0.488	Cr	3339
MgO	18.761	Cu	25
Na2O	0.074	Mo	56
TiO2	0.041	Ni	32905
MnO	0.044	Sr	44
P2O5	0.131	V	22626
SO3	25.5	Zn	507
TOC	7.46733	Zr	46
LOI	8.26657	La	13
-	-	Pb	21

2.2.Preparation of Composites

The YOFA powders, as received, were first ground using an electrical powder grinder at a speed of 25000 rpm for 15 minutes to achieve a wide range of particle sizes. The powder was then sieved to obtain four grades of particle size: YOFA 1 (53-80 µm), YOFA 2 (80-125 µm), YOFA 3 (125-150 µm), and YOFA 4 (150-250 µm). HDPE and YOFA were dried at 80°C for 8 hours to eliminate moisture and other volatile substances. To ensure better mixing of YOFA in the HDPE matrix during melt blending (extrusion), both materials were manually mixed in the presence of an acetone solvent, as shown in Fig. 1. The YOFA particles get coated on the surface of HDPE granules due to the solvent's presence, as Verma et al. [24] suggested and offered. To prepare HDPE/YOFA composites, a mixture filament was obtained by melt blending using a single-screw extruder, specifically a SJ25 plastic extruder. The extruder was equipped with a screw of 25 mm in diameter and an L/D ratio of 16. The temperature in the first, second, and third zones was maintained at 40°C, 150°C, and 140°C, respectively, from the feeding zone to the mold exit. The screw speed was set between 9 and 11 r.p.m. Five mixtures of HDPE/YOFA composites were prepared separately by mixing YOFA particles at concentrations ranging from 0 to 8 wt.% in 2% increments. As shown in Table 2, the samples were designated as HXFY, where X is the content of YOFA, and Y is the particle size grades. In contrast, pure HDPE is labeled as NHD.

Table 2 The Sample Labels at Different Particle Size Grades and YOFA Content.

YOFA (wt.%)	YOFA 1 (53-80 µm)	YOFA 2 (80-125 µm)	YOFA 3 (125-150 µm)	YOFA 4 (150-250 µm)
0	NHD	NHD	NHD	NHD
2	H2F1	H2F2	H2F3	H2F4
4	H4F1	H4F2	H4F3	H4F4
6	H6F1	H6F2	H6F3	H6F4
8	H8F1	H8F2	H8F3	H8F4

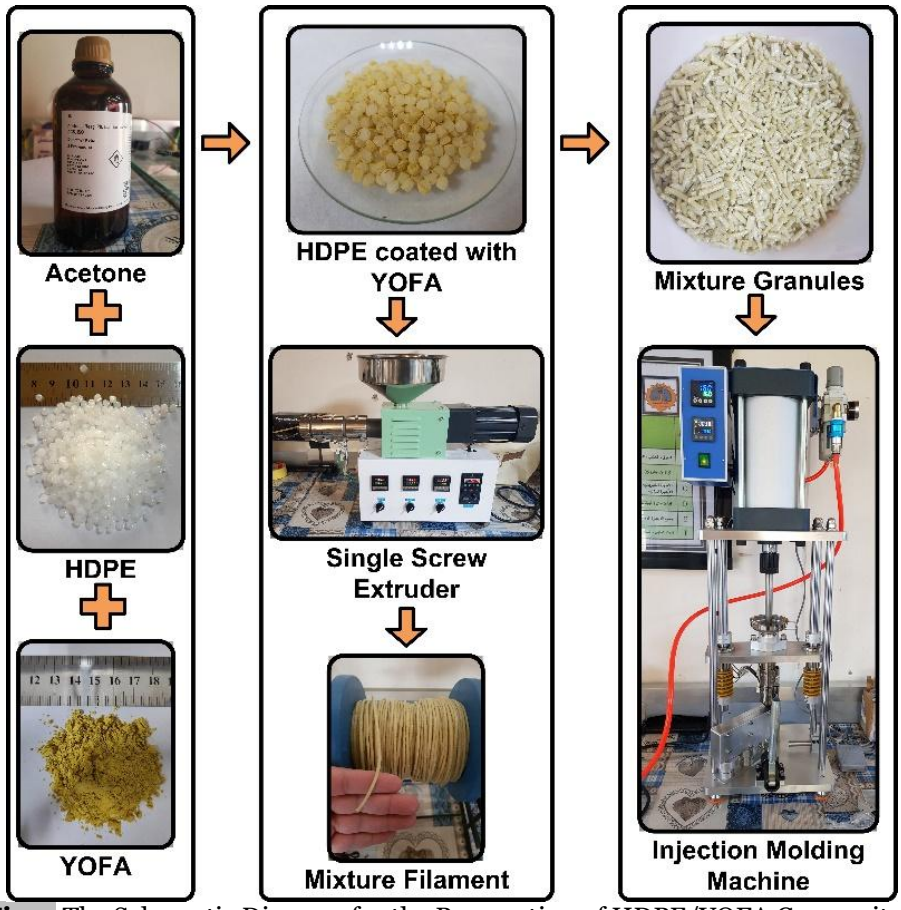

Fig. 1 The Schematic Diagram for the Preparation of HDPE/YOFA Composites.

After extrusion, the filament mixture was cut into granules using an electric cutter. These granules were then molded using a vertical plastic injection molding machine, XCX-40G, to produce test specimens after a pilot study to achieve the typical parameters. All mixture granules of HDPE/YOFA composites were dried for 2 hours at 80°C before injection molding to eliminate any moisture retained from the extrusion process. Table 3 shows the typical parameters of the injection molding machine.

Table 3 The Typical Parameters of the Injection Molding Machine.

Typical parameters	
Injection temperature	160 °C
Holding temperature time	6-8 min
Injection pressure	0.6 MPa
Holding pressure time	30 s
Injection time	1 s
Mold temperature	23+2 °C
Cooling time	1-2 min

2.3.Physical and Mechanical Properties

In this study, several physical and mechanical properties were examined and analyzed. The experimental density (ED) of HDPE/YOFA samples was determined using Archimedes' principle, specified in ASTM Standard D792-20 [25]. To achieve this, a Sartorius high-sensitivity balance with a precision of 0.1 mg was used. Prior to the measurements, all samples were dried at 80°C for 4 hours. To calculate the density of the composites, the specimen was first weighed in air. Next, the specimen was weighed while immersed in distilled water at 23°C, using a sinker and wire to hold it wholly submerged. Before taking the measurement, care was taken to ensure that no air bubbles were trapped. Three specimens per batch were assessed, and the average was calculated as the composite ED. Eq. (5) was utilized to determine the ED of YOFA/HDPE composites at 23 °C [25–27]:

$$\mathbf{ED} = \left(\frac{\mathbf{A}}{\mathbf{A+S-B}}\right) * \mathbf{0.9978} \qquad \mathbf{(5)}$$

Here, A represents the mass of a dry specimen in the air without the sinker, while B is the mass of the specimen and sinker when they are completely immersed, along with the wire partially immersed in gas-free distilled water at 23 °C. On the other hand, S is the mass of the immersed sinker and partially immersed wire. It is important to note that the density of water at 23 °C is 0.9978 g/cm^3. Theoretical density (TD) and void content (VC) were calculated using the mixture rule according to ASTM D2734 [28] by utilizing Eqs. (6) and (7), respectively:

$$\mathbf{TD} = \frac{\mathbf{100}}{\frac{\mathbf{R}}{\mathbf{D}} + \frac{\mathbf{r}}{\mathbf{d}}} \qquad \mathbf{(6)}$$

Where R is HDPE's weight percentage, D is HDPE's density, r is the weight percentage of YOFA, and d is the density of YOFA.

$$\mathbf{VC} = \frac{\mathbf{100\ (TD - ED)}}{\mathbf{TD}} \qquad \mathbf{(7)}$$

An HDPE/YOFA composite's water absorption (WA) test and thickness swelling (TS) were conducted following ASTM D570 [29]. The specimens were dried at 80°C in an oven until a constant weight was achieved. The weight and thickness of the dried samples were measured with a precision of 0.1 mg and 0.001 mm, respectively. They were then submerged in a bath of distilled water. The specimens were removed after 7 days of immersion; the surface water was wiped off with blotting paper. Then, their wet mass values and thickness were measured. Eqs. (8) and (9) calculated the values of WA and TS, respectively [29, 30]:

$$\mathbf{WA} = \frac{\mathbf{W-A}}{\mathbf{A}} * \mathbf{100} \qquad \mathbf{(8)}$$

where W represents the specimen's wet mass after 7 days of immersion, and A represents its dry mass.

$$\mathbf{TS} = \frac{\mathbf{T_w - T_d}}{\mathbf{T_d}} * \mathbf{100} \qquad \mathbf{(9)}$$

where Tw and Td denote the thickness of the specimen after 7 days of immersion and the specimen's dry thickness, respectively. Shore D Hardness of the samples was measured at room temperature using a Hardness Tester (Durometer) according to ASTM D2240 [31]. Three samples were taken, and an average of five values was reported for each sample. The corresponding standard deviations have also been reported. The measurements commenced ten seconds after the durometer tip made contact with the sample. According to ASTM G99-17 [32], a dry sliding wear test was conducted at room temperature using an ED-201 pin-on-disc tribometer, manufactured by Ducom, Bangalore, India. The test involved placing a sample with a diameter of 5 mm and a height of 20 mm in a holder against a steel disc with a hardness of 62 HRC. Both the sample and the counter steel disc were cleaned with acetone before and after each period of the dry wear test. The steel disc and sample ends were ground with grade 1000 emery paper to maintain the uniform surface roughness of the samples during the entire experiment. The test parameters, including applied loads, sliding time, sliding distance, sliding velocity, and disc diameter, are listed in Table 4. The loads applied to the samples were connected vertically and directly to their longitudinal direction through the device design. After each test, the steel disc counter was allowed to cool to room temperature and then cleaned with organic solvents to remove any wear debris stuck on its surface. The samples were weighed before and after each test to determine and calculate the wear loss using the balance with a precision of 0.1 mg. The wear rate was calculated by dividing the wear loss by the sliding distance. Three samples were tested for each composite composition to determine the average wear rate. Wear tests were conducted at a room temperature of 23±2 °C and a relative humidity of 35%. The morphology of the worn surfaces and wear tracking were investigated via SEM. This morphological study examines the wear process and its underlying sub-mechanisms responsible for surface damage. The flowchart of the experimental procedure sequence for manufacturing HDPE/YOFA composites is presented in Fig. 2.

Table 4 The Factors of the Dry Sliding Wear Test.

Factors	Levels
Applied loads	5, 10, 15, and 20 N
Sliding time	5, 10, 15, and 20 min
Sliding distance	452.4, 904.8, 1357.2, and 1809.6 m
Disc velocity	480 r.p.m
Sliding velocity	1.5 m/s
Disc diameter	6 cm

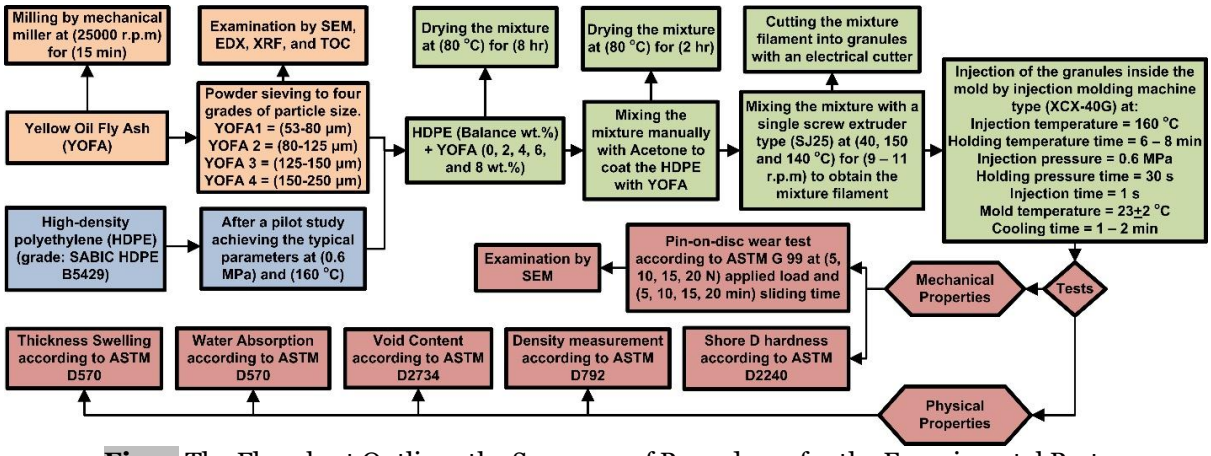

Fig. 2 The Flowchart Outlines the Sequence of Procedures for the Experimental Part.

2.4.Design of Experiment Method

Dry sliding wear depends on the characteristics of the contact conditions and tribo-pairs. Therefore, it is necessary to clarify the influence of each parameter and the interactions that affect the abrasive wear of composites. The Design of Experiments (DOE) method is a valuable technique for optimizing complex testing procedures. It is helpful to obtain knowledge about the optimal levels of various parameters by considering multiple factors. Full-factorial design (FFD) is a crucial aspect of DOE as it enables the calculation of overall interactions and the main effects of different test factors. Every parameter setting appears with every other one when using an FFD analysis [33–35]. The FFD is a combination of mathematical and statistical methods used to model and analyze problems where multiple variables influence a response of interest, to optimize that response. In factorial problems, the relationship between the response and independent variables is often unknown. Therefore, the first step in factorial design is to approximate the true functional relationship between the response of interest (y) and a set of independent variables. Besides, the Taguchi technique was used to calculate the signal-to-noise ratio (S/N). The Taguchi technique is a popular statistical method used for planning trials. It helps in analyzing deviations from the intended functional value to improve operations. Implementation of FFD and Taguchi analysis are used to optimize factors influencing dry sliding wear [33–35]:

1) As per the procedure, an FFD of the experiment and the Taguchi method have been implemented for designing the experimental trials. Statistical software tools, such as MINITAB 21 and Microsoft Excel, are employed for error-free computations and manually cross-verified for accuracy.

2) An FFD analysis was conducted to examine the tribological behavior of the composites. To understand the dry sliding wear process, it is essential to identify the factors that affect it. Four factors, including the YOFA compositions, the YOFA particle size, the applied normal load, and the sliding time, were selected to characterize the wear properties of the samples. These factors are essential parameters in wear tests that impact composite performance. Experts and literature have been consulted to determine the appropriate levels of these factors, which are tabulated in Table 5. It is also important to note the output response, specifically the wear loss and wear rate of the polymeric composites. The sliding velocity was maintained at a constant rate (1.5 m/s), effectively controlling debris removal from the interface region. Accordingly, a general FFD was selected, and an L320 standard orthogonal array was utilized. It had four columns and 320 rows, resulting in 319 degrees of freedom to manipulate four parameters with multiple levels, as shown in Table 5. Thus, 320 experiments were conducted to test wear using various combinations of four parameters: two intrinsic and two extrinsic, assigned to the columns and rows, respectively.

3) The FFD method was used to analyze variance (ANOVA) to optimize the control parameters and determine their order of significance in the dry sliding wear process. The ANOVA tool would serve as a cross-check to validate the order of significance of the input control parameters. The ANOVA is useful for estimating error variance and determining the contribution percentages of the parameters. It is primarily designed for statistical analysis and optimizing output responses.

4) In the Taguchi method, the designer selects two types of factors: control factors and noise factors. Control factors are factors that the designer can control, as presented in Table 5. In contrast, noise factors are uncontrollable factors that can cause deviations from the desired outcome, such as temperature fluctuations and human error. Controlling all noise and uncontrollable factors, such as temperature, humidity, and air movement, is crucial for performing all experiments simultaneously under controlled laboratory conditions. The Taguchi method uses the S/N ratio as a metric to assess a system's performance. The S/N ratio measures the variation of quality parameters from their target values, which can help to maximize desired features and minimize variability in a process or product. There are two common types of S/N ratios: the higher-the-better (HTB) S/N ratio and the smaller-is-optimal (SIO) S/N ratio. The choice of S/N ratio depends on whether the goal is to enhance or reduce a response [34]. The main objective of this investigation is to improve wear resistance. To achieve this, it is essential to consider that smaller is better. The maximum S/N ratio minimizes the average square error loss in simulated process models. This ratio utilizes specific design parameters, making it easier to break the parameter design optimization procedure into two smaller, more manageable optimization steps. Eq. (6) below was used to calculate the S/N ratio for wear properties and determine the effect of various factors and their interactions, using the "smaller the better" formulation to analyze test data [33, 35].

$$\frac{S}{N} = -10 \log \frac{1}{n} (\sum y^2) \qquad (10)$$

where S/N represents the signal-to-noise ratio, n represents the number of observations, and y

represents the respective characteristic. Several noise factors can affect the experimental results in the wear testing of HDPE/fly ash composites. Variability in fly ash content, such as uneven distribution within the composite, can lead to inconsistencies in wear resistance. Differences in fly ash particle size and shape may also introduce variability in wear behavior. Additionally, slight fluctuations in the applied normal load during the test could affect the wear rate. At the same time, environmental factors such as temperature changes or variations in surface roughness over time may influence the results during extended periods of sliding. Controlling these noise factors is essential for ensuring accurate and reliable outcomes.

Table 5 The Different Levels of Factors Used in a Full-Factorial Experimental Design and the Taguchi Method.

No.	Factor/parameter	Level 1	Level 2	Level 3	Level 4	Level 5
1	A: YOFA content (%)	0	2	4	6	8
2	B: Particle Size of YOFA (µm)	1	2	3	4	-
3	C: Applied Normal Load (N)	5	10	15	20	-
4	D: Sliding Time (min)	5	10	15	20	-

3.RESULTS AND DISCUSSION

3.1.SEM/EDX Analysis of YOFA

SEM examination was used to observe the surface morphology, shape, and size of YOFA particles, and EDX was utilized to determine their elemental content. Figures 3-6 display SEM images and EDX of YOFA particles for different grades: YOFA 1 (53-80 µm), YOFA 2 (80-125 µm), YOFA 3 (125-150 µm), and YOFA 4 (150-250 µm). The SEM images clearly show the dendritic and irregular shapes of YOFA particles, as well as their dimensions. EDX analysis data show that YOFA particles have high C, O, Mg, S, and V concentrations in their content.

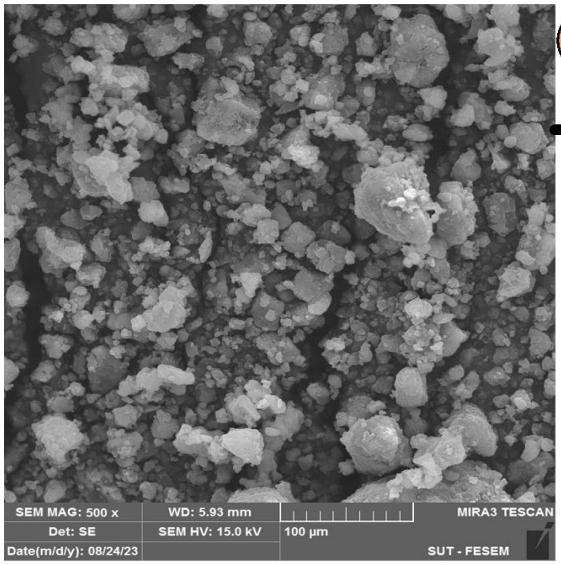

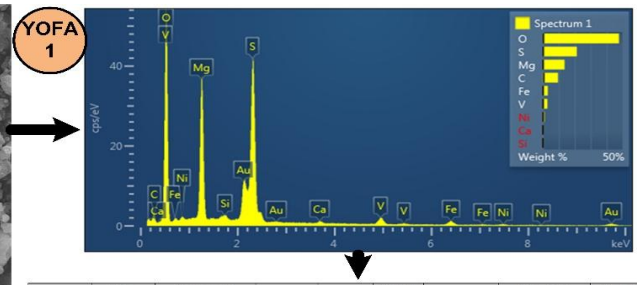

Element	Line Type	Apparent Concentration	K Ratio	Wt.%	Wt.% Sigma	Atomic %	Standard Label	Factory Standard
C	K series	0.34	0.00337	9.49	0.57	15.32	C Vit	Yes
O	K series	15.09	0.05079	47.78	0.39	57.93	SiO2	Yes
Mg	K series	4.41	0.02927	13.59	0.15	10.85	MgO	Yes
Si	K series	0.14	0.00113	0.43	0.05	0.30	SiO2	Yes
S	K series	6.87	0.05914	21.29	0.21	12.88	FeS2	Yes
Ca	K series	0.15	0.00133	0.45	0.06	0.22	Wollastonite	Yes
V	K series	0.78	0.00782	2.84	0.11	1.08	V	Yes
Fe	K series	0.86	0.00860	3.06	0.16	1.06	Fe	Yes
Ni	K series	0.30	0.00304	1.08	0.18	0.36	Ni	Yes
Total:				100.00		100.00		

Fig. 3 SEM Image and Elemental Content (EDX) for YOFA 1.

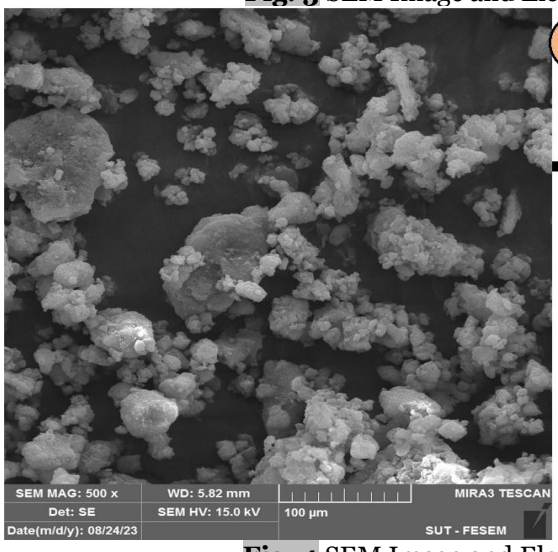

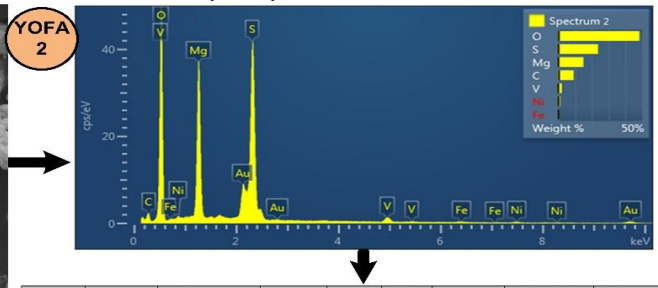

Element	Line Type	Apparent Concentration	k Ratio	Wt.%	Wt% Sigma	Atomic %	Standard Label	Factory Standard
C	K series	0.41	0.00405	10.75	0.51	15.94	C Vit	Yes
O	K series	12.6	0.04240	48.40	0.36	58.85	SiO2	Yes
Mg	K series	4.46	0.02959	11.3	0.22	9.52	MgO	Yes
S	K series	6.87	0.05914	21.29	0.21	12.88	FeS2	Yes
V	K series	2.09	0.02090	6.58	0.17	2.30	V	Yes
Fe	K series	0.13	0.00134	0.41	0.11	0.13	Fe	Yes
Ni	K series	0.41	0.00412	1.27	0.16	0.38	Ni	Yes
Total:				100.00		100.00		

Fig. 4 SEM Image and Elemental Content (EDX) for YOFA 2.

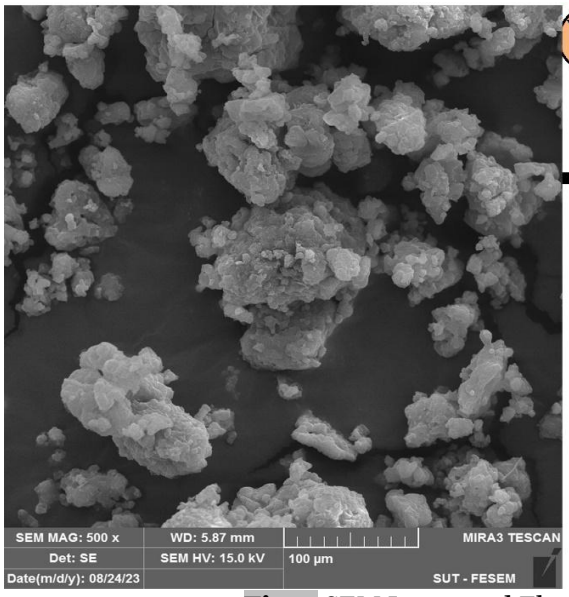

Element	Line Type	Apparent Concentration	K Ratio	Wt.%	Wt.% Sigma	Atomic %	Standard Label	Factory Standard
C	K series	0.27	0.00271	9.13	0.50	14.59	C Vit	Yes
O	K series	13.88	0.04670	48.38	0.36	58.04	SiO2	Yes
Mg	K series	4.48	0.02970	14.95	0.15	11.80	MgO	Yes
S	K series	6.90	0.05940	23.74	0.21	14.21	FeS2	Yes
V	K series	0.52	0.00518	2.10	0.11	0.79	V	Yes
Fe	K series	0.14	0.00139	0.55	0.13	0.19	Fe	Yes
Ni	K series	0.29	0.00290	1.15	0.18	0.37	Ni	Yes
Total:				100.00		100.00		

Fig. 5 SEM Image and Elemental Content (EDX) for YOFA 3.

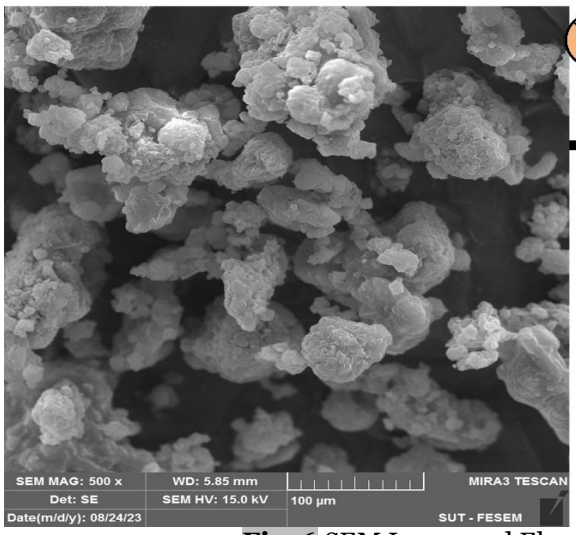

Element	Line Type	Apparent Concentration	K Ratio	Wt.%	Wt.% Sigma	Atomic %	Standard Label	Factory Standard
C	K series	0.22	0.00225	8.16	0.49	13.22	C Vit	Yes
O	K series	12.60	0.04240	48.40	0.36	58.85	SiO2	Yes
Mg	K series	3.99	0.02647	14.53	0.14	11.63	MgO	Yes
S	K series	6.38	0.05498	23.75	0.22	14.41	FeS2	Yes
V	K series	0.71	0.00711	3.12	0.12	1.19	V	Yes
Fe	K series	0.24	0.00244	1.05	0.14	0.37	Fe	Yes
Ni	K series	0.23	0.00230	0.98	0.19	0.33	Ni	Yes
Total:				100.00		100.00		

Fig. 6 SEM Image and Elemental Content (EDX) for YOFA 4.

3.2.Physical Characterizations Analysis

Figure 7 shows the relation between the content and particle size of YOFA particles with the density, void content, water absorption, and thickness swelling of HDPE composites. As can be observed in Fig. 7 (a), the theoretical densities of the YOFA-filled HDPE composites increased by 4.7%, with the YOFA content increasing from 0 to 8 wt.%. In contrast, the actual or experimental densities increased positively with the YOFA content by 4.24%, 4.23%, 4.1%, and 3.9% for YOFA 1, YOFA 2, YOFA 3, and YOFA 4, respectively. Both densities showed an increasing linear trend, with YOFA content in the composite compositions. This behavior is evident due to the increased presence of a denser YOFA phase (2.18 g/cc) compared with HDPE (0.954 g/cc). Adding YOFA to HDPE resulted in a more viscous melt, requiring higher temperatures and injection pressures, which made processing difficult. However, as expected, the composite's shrinkage ratio decreased with the increase in fly ash content. Theoretical densities are consistently higher than actual densities. This discrepancy is apparent because theoretical calculations are based on the idealistic assumptions of (i) a material state free of defects or imperfections and (ii) fabrication and processing conditions executed with flawless instrumentation. Practically, materials often have defects or imperfections, such as agglomerations and non-uniform dispersions. Hidden errors in the fabrication process and processing conditions, which would stem from improper instrumentation or human mistakes, can reduce the effectiveness of theoretical densities [33]. The differential thermal expansion coefficients of YOFA and HDPE would create voids during temperature changes, affecting the composite's density. Conversely, the experimental density showed a negative correlation with the increase in particle size for all YOFA content, exhibiting a slight and gradual decrease as the particle size of YOFA increased. The size and distribution of YOFA particles within the HDPE matrix are critical in determining the composite's actual

density. Non-uniform dispersion or agglomeration of YOFA particles can result in voids and a declining density. The reasons for a reduction in density with increasing particle size would be attributed to several factors, which include:

1) Inadequate Packing Efficiency: The larger YOFA particles might not be as densely packed within the HDPE matrix as the smaller ones, resulting in gaps or voids among the particles, potentially reducing the composite's experimental density.
2) Increased Interparticle Spaces: The larger YOFA particles generally exhibit wider gaps between them, leading to a higher volume fraction of voids within the composite material. This increase in void content contributes to the reduced density.
3) Reduced Dispersion: The larger YOFA particles might not disperse evenly throughout the HDPE matrix during manufacturing. This dispersion can lead to agglomeration or clustering, resulting in areas of low density within the composite.

The term 'porosity' or 'voids' refers to the relative measure of differences between actual and theoretical densities. A high void fraction should be avoided, as it can undermine the product's value engineering. Figure 7 (b) corroborates the previously mentioned findings. The void content rises significantly with an increase in both the reinforcement content and the particle size. The bonding nature and shape of all reinforcing phases in the specimens examined in this study are consistent, except for their proportion and size. Additionally, the proportion of the matrix diminishes as the reinforcing phase increases in a mixture design. A mix design with a lower proportion of the reinforcing phase and, consequently, a higher content of the matrix phase exhibits reduced viscosity during fabrication due to the greater matrix proportion relative to the reinforcing phases. The presence of bubbles, which would vary in quantity, is contingent upon the sample maker's expertise and the artistry involved. These bubbles can infiltrate the material during the curing phase of fabrication. Moreover, as the reinforcing phase content in a mixture increases, so does the viscosity, leading to a higher chance of porosity or voids during fabrication. As viscosity increases, the ability of gases to escape during solidification decreases, making it more likely that the gases will be trapped in the sample, increasing the voids. Concurrently, due to the increased content of reinforcing phases, the matrix encounters fewer surface sites to glue to, potentially elevating the occurrence of voids. This behavior continues with increases in the content and particle size of reinforcement. On the other hand, Table 1 indicates the considerable presence of sulfur (30.24%) and sulfites (25.5%) in the YOFA content, which causes a weak physical bond between HDPE and YOFA particles [36], thereby increasing the void content. Consequently, composites with lower content and smaller particle sizes are anticipated to exhibit stronger interface bonding due to their increased continuity and minimal void presence. When subjected to external loads, most stress is promptly transferred to the reinforcing phase, leaving only a minimal portion for the matrix phase to absorb. This approach prevents catastrophic failure in the matrix phase, enhancing the material's mechanical and thermal properties. Consequently, these composite materials are well-suited for structural, mechanical, or tribological applications. Deviations from the standard can lead to a degradation of material properties, as an increased presence of voids serves as an internal stress concentrator, which can exacerbate the straining effect even under lower loads. Water sensitivity is a crucial criterion for the practical applications of polymer composite products. It is known that water absorption significantly impacts the long-term strength of the polymer matrix [27, 37]. Figures 7 (c) and (d) illustrate the correlation between water absorption and thickness swelling regarding particle size and the content of YOFA, respectively. Both water absorption and thickness swelling significantly increased with the increase in the content and particle size of YOFA particles. Water absorption increased significantly with the YOFA content, rising by 94%, 101.5%, 103.5%, and 111.5%, respectively. The thickness swelling also increased, by 142.5%, 148%, 239.5%, and 241.2% for YOFA 1, YOFA 2, YOFA 3, and YOFA 4, respectively. This behavior aligns perfectly with the linearly increasing trend of void content, as shown in Fig. 7 (b), indicating that any rise in water absorption and thickness swelling is attributed to the content of voids. Increasing the number of voids increases the chance of water infiltration, thereby maximizing the risk of dimensional changes in parts during operation and increasing the risk of malfunctions or part failures. The opposite is also true. This rise in water absorption and thickness swelling can be attributed to the larger particle sizes and the hydrophilic nature of YOFA, resulting from the high hygroscopicity of its chemical constituents.

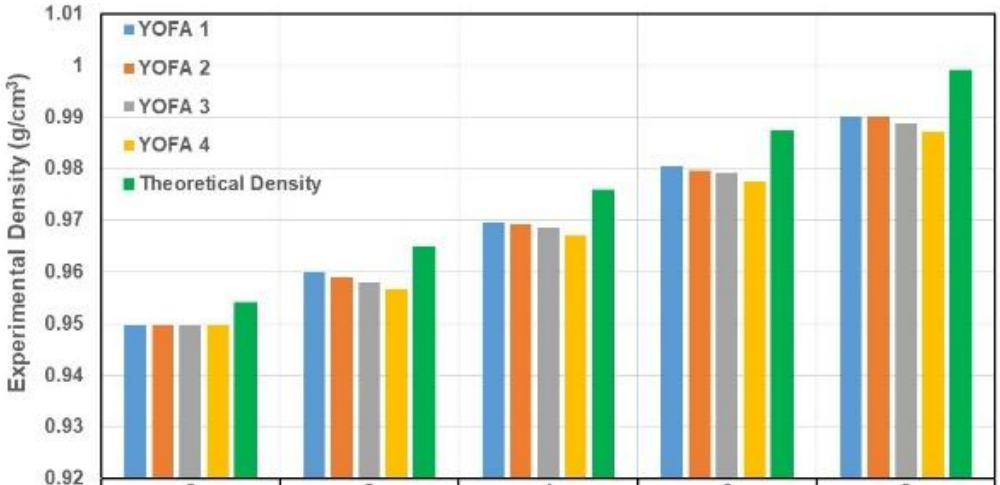

	0	2	4	6	8
YOFA 1	0.949824585	0.960019679	0.969547811	0.980360283	0.990139592
YOFA 2	0.949824585	0.958951495	0.969279696	0.979562695	0.990038643
YOFA 3	0.949824585	0.958031557	0.968681409	0.979349119	0.988675787
YOFA 4	0.949824585	0.956745098	0.96703513	0.977447463	0.987246762
Theoretical Density	0.954	0.964859242	0.975968548	0.987336658	0.99897272

YOFA Content (%)

(a)

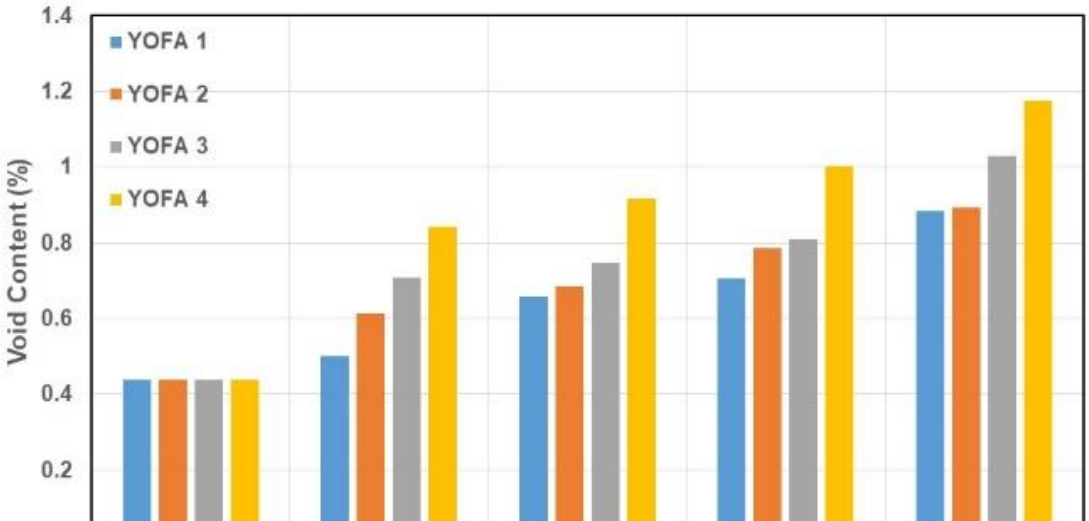

	0	2	4	6	8
YOFA 1	0.437674567	0.50158229	0.657883581	0.706585219	0.884221214
YOFA 2	0.437674567	0.612291026	0.685355317	0.787366928	0.894326429
YOFA 3	0.437674567	0.707635291	0.746657197	0.808998497	1.030752182
YOFA 4	0.437674567	0.840966566	0.915338755	1.001603113	1.17380166

YOFA Content (%)

(b)

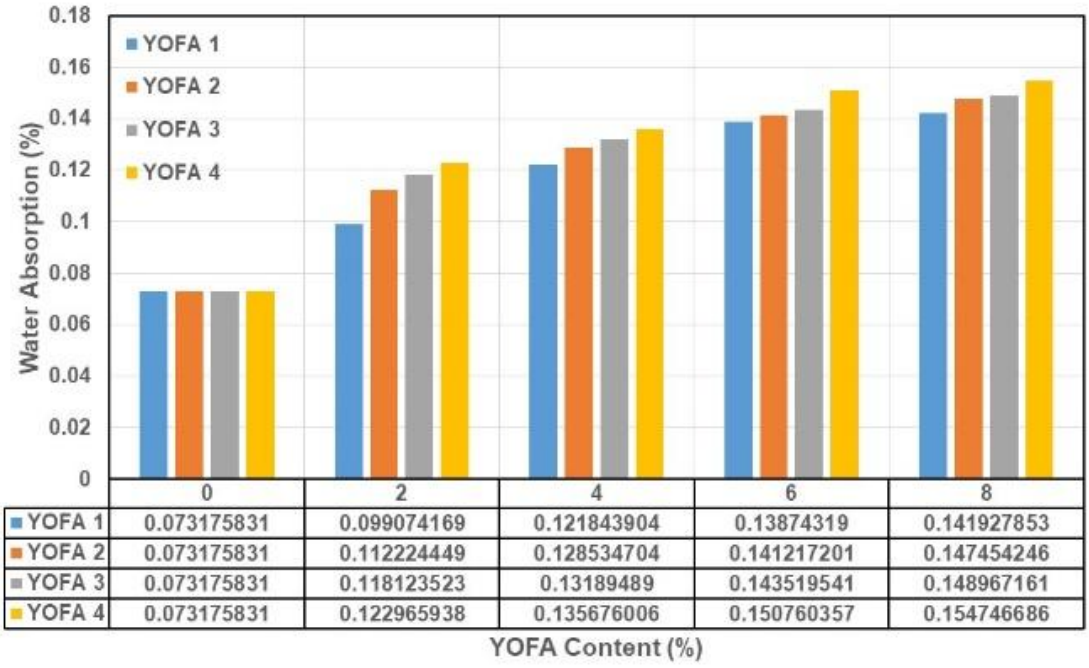

	0	2	4	6	8
YOFA 1	0.073175831	0.099074169	0.121843904	0.13874319	0.141927853
YOFA 2	0.073175831	0.112224449	0.128534704	0.141217201	0.147454246
YOFA 3	0.073175831	0.118123523	0.13189489	0.143519541	0.148967161
YOFA 4	0.073175831	0.122965938	0.135676006	0.150760357	0.154746686

(c)

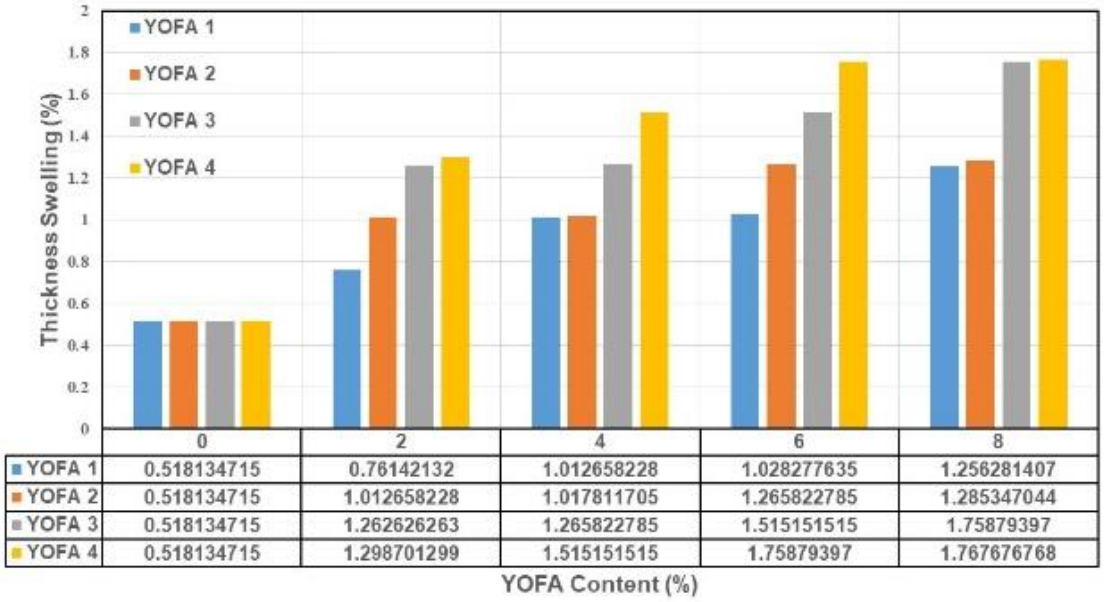

	0	2	4	6	8
YOFA 1	0.518134715	0.76142132	1.012658228	1.028277635	1.256281407
YOFA 2	0.518134715	1.012658228	1.017811705	1.265822785	1.285347044
YOFA 3	0.518134715	1.262626263	1.265822785	1.515151515	1.75879397
YOFA 4	0.518134715	1.298701299	1.515151515	1.75879397	1.767676768

(d)

Fig. 7 Physical Properties Result from HDPE/YOFA Composites: (a) Density, (b) Void Content, (c) Water Absorption, and (d) Thickness Swelling.

3.3.Hardness Characterization Analysis

Hardness measures a material's integrity and its resistance to penetration under point loading [33]. In other words, hardness typically refers to a material's resistance to surface indentation, scratching, or marring [38, 39]. Figure 8 demonstrates the relationship between the concentration and particle size of YOFA particles with shore D hardness for the HDPE matrix composites. The hardness values exhibited a slight and linear decrease with the rising concentration and particle size of YOFA content in the HDPE matrix, showing reductions of 11%, 11.5%, 13.6%, and 17.3% for YOFA 1, YOFA 2, YOFA 3, and YOFA 4, respectively. The slight reduction in the hardness values of the composites is deemed acceptable for their application in engineering contexts. The observation is precise in all compositions. The ingredients are the same and produced under the same process conditions; therefore, factors such as material properties, randomness, bond strength, phases, and shape are consistent. Consequently, the interface's nature, strength, proportion, size, and distribution are the main factors influencing the resulting properties. The decrease in hardness value can be primarily attributed to the increased void content in HDPE/YOFA

composites, as shown in Fig. 7 (b). The presence of voids significantly influences the mechanical properties of materials. The fewer the voids, the greater the continuity of the matrix phase, thereby enhancing the load transfer mechanism from the matrix to the reinforcing phase, which bears the majority of the load. Consequently, this increases the mechanical and thermal properties of the composite specimens. Voids serve as internal stress concentrators that can cause catastrophic failure of the matrix phase under minimal external loading, thereby reducing the mechanical and thermal properties of the composites [33]. Earlier studies by Chand et al. [40] and Nasir et al. [11] have confirmed the same findings: the hardness of HDPE matrix composites decreases with increasing concentration of coal FA. The hardness reduction achieved by increasing the concentration and particle size of the YOFA content can be summarized as:

1) The interaction between YOFA particles and the HDPE matrix plays a crucial role in determining the hardness of the composite. If the particle size is too large or the content is too high, it can weaken the interaction, resulting in a decrease in hardness. This decrease occurs because the larger particles are not well bonded to the matrix, and a higher content can cause particle agglomeration, which disrupts the matrix continuity. The strength of the bond between YOFA particles and the HDPE matrix is significant for achieving hardness. When the particle size increases, the surface area available for bonding decreases relative to the volume. This behavior could weaken the bond's strength between the particles and the matrix, reducing its hardness.

2) The hardness of a composite material depends on the effectiveness of the load transfer from the HDPE matrix to the YOFA particles. However, suppose the YOFA particles are larger and more numerous. In that case, they would impede this process as they can act as stress concentrators instead of stress distributors, mainly if there is inadequate interfacial adhesion. Larger particles of YOFA can cause localized stress concentrations, resulting in an uneven stress distribution that does not contribute to composite hardness.

3) Thermal mismatch refers to the differences in thermal expansion coefficients between HDPE and YOFA, which can result in internal stresses caused by temperature changes. When larger particles are present, they have a higher potential to create these stresses due to their size, which can cause micro-cracking and a decrease in hardness.

4) Morphological changes are essential in determining a composite material's hardness, including the distribution, shape, and size of YOFA particles within the HDPE matrix. Due to the uneven distribution of particles or irregular shapes, non-uniform stress distribution and localized weakening can occur. Therefore, the composite's morphology should be considered for optimal performance. Particle agglomeration at higher YOFA content can weaken the matrix by creating less effective load transfer than well-dispersed particles.

5) As previously stated, larger YOFA particles can increase the void content in the composite. These voids are essentially defects in the material that can significantly reduce hardness by providing easy paths for crack initiation and propagation.

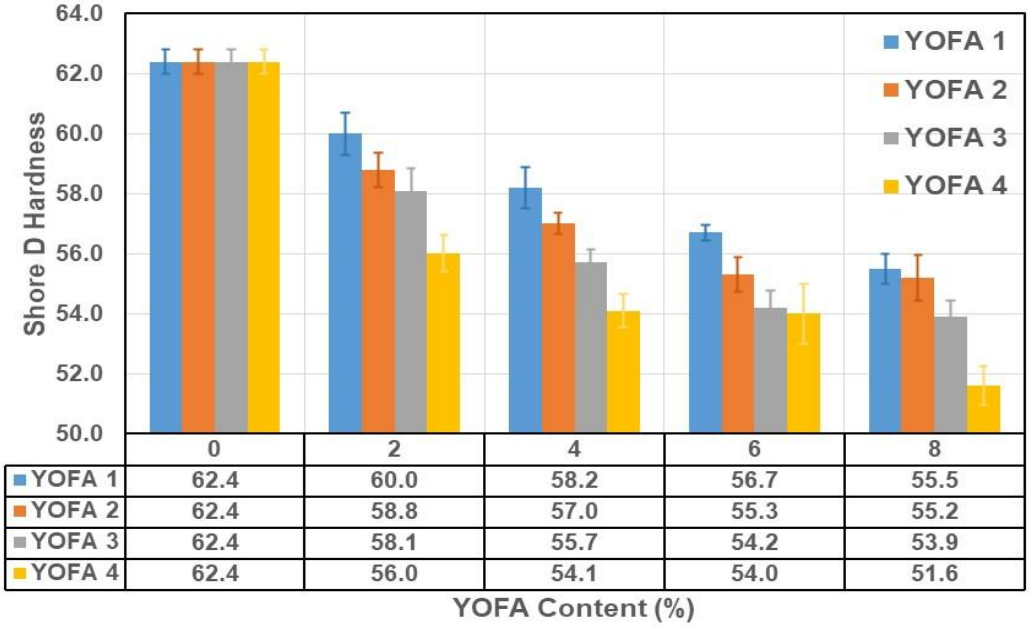

	0	2	4	6	8
YOFA 1	62.4	60.0	58.2	56.7	55.5
YOFA 2	62.4	58.8	57.0	55.3	55.2
YOFA 3	62.4	58.1	55.7	54.2	53.9
YOFA 4	62.4	56.0	54.1	54.0	51.6

Fig. 8 Relationship Between the Concentration and Particle size of YOFA Content with Shore D Hardness for the HDPE Matrix Composites.

3.4.Dry Sliding Wear Characterization Analysis

Figures 9 and 10 display the main and interaction effect plots for wear loss and wear rates in HDPE/YOFA composites under different wear factors. In other words, these Figures provide the correlation between the wear loss and wear rates of the HDPE/YOFA composites with different particle sizes and YOFA content concentrations under varying wear factors, as tabulated in Table 5. The mechanical and wear characteristics of polymer composites depend on the type, shape, size, and content of the filler and chemical treatment. These factors play an essential role in determining the performance of the composites [35]. The Pin-on-disc method was utilized to determine the wear rate of HDPE/YOFA composites at room temperature. The test was conducted under varying applied normal loads and sliding times. The wear rate was measured based on the amount of debris dislocated from the composites. It is important to note that the wear rate is inversely proportional to the wear resistance. During the wear test, the sample surface initially adheres directly to the disc surface with no separation. Then, as the hard counter disc generates a shear force, the sample surface deforms, and particles dislocate from the sample, forming wear debris. The presence of this debris between the tribosurfaces during sliding acts as an abrasive medium, altering the wear mechanism from a two-body wear mechanism to a three-body wear mechanism [41]. Figures 9 and 10 exhibit several trends that can be observed as:

1) **Effect of YOFA Concentration on Wear Test**

   Both wear loss and wear rate increased slightly with an increase in the YOFA concentration of up to 2%. Then, they decreased gradually and linearly with increasing YOFA content. The slightly increased wear rates associated with higher YOFA content would be due to the increased rigidity of the structure, which causes greater abrasive wear between samples and counterparts. Additionally, this decrease in wear resistance can be attributed to the reduction in composite hardness with increasing YOFA concentration, as shown in Fig. 8, as well as the increase in void content, as illustrated in Fig. 7 (b), which leads to a slight rise in wear rate. The evident improvement in wear resistance after 2% YOFA concentration is attributed to several factors. XRF spectrometry analysis was conducted on YOFA particles, as shown in Table 1. The analysis revealed that oxides, sulfur, sulfites, and other minerals were present in significant amounts in the YOFA content. The presence of oxides and other materials in YOFA has improved its wear resistance. This improvement can be attributed to the rigidity of oxides and other content in YOFA. Generally, ash particles tend to reduce the coefficient of friction, leading to increased wear resistance. The ash particles are believed to act as barriers, preventing the composite matrix from fragmenting. Furthermore, the high concentration of sulfur, sulfites, and other minerals found in YOFA content results in the creation of a small lubricant film that exists between the surfaces that come into contact with each other (also known as tribosurfaces). This lubricating film alters the nature of the contact surfaces from polymer to metal, separating the tribosurfaces by a thin lubricating film, which helps minimize direct contact between the HDPE/YOFA composites and the counterface. As a result, the wear rate of the composites decreases. Moreover, the surface shape of YOFA particles is irregular and dendritic, as presented in Figs. 3-6, which creates a larger contact area and enhances adhesion with the HDPE matrix, improving bonding at the interface, decreasing the likelihood of particle pull-out and matrix cracking during wear, and ultimately leading to reduced wear rates. Improvement of YOFA content leads to a drastic enhancement in the experimental density of composites, as shown in Fig. 7 (a), which reduces the penetration of abrasive particles during wear, thereby decreasing the wear rate. Finally, the distribution and dispersion of YOFA particles within the HDPE matrix are important for wear resistance. If the particles are uniformly dispersed throughout the composite, the load is distributed evenly, preventing localized wear. A uniform particle distribution also improves the composite's resistance to crack propagation, ultimately reducing wear rates. Additionally, Alshabander et al. [15] found that increasing the CFA concentration in RHDPE significantly decreased the wear rate. Additionally, Ramanjaneyulu et al. [42] reported that the wear rate decreased significantly with the addition of oxide particles in HDPE matrix composites.

2) **Effect of YOFA Particle Size on Wear Test**

   As YOFA particle sizes increased, wear loss and wear rates increased significantly for all other factors. The reduction in wear resistance can be mainly attributed to two factors. The first factor is the rise in void content as the particle size of YOFA increases, as shown in Fig. 7 (b), where voids represent the areas of stress concentration, leading to the formation of more cracks and dislocation of the YOFA

particle during the wear test. The second factor is the deterioration in composite hardness with increasing YOFA particle size, as shown in Fig. 8, due to the wear rates being inversely proportional to the hardness of the composite, as indicated by Archard's law [43, 44], which accurately describes the relationship between wear loss and other factors, as shown in Eq. (11):

$$W = K\frac{NS}{CH} \quad (11)$$

where W, H, S, N, K, and C represent wear loss, hardness, sliding distance, applied normal load, constant of wear, and geometrical microstructure factor, respectively. Archard's law states that a decrease in hardness reduces wear resistance, as it decreases the contact force between particles, thereby facilitating severe contact between tribosurfaces. On the other hand, wear debris is generated at the lower particle sizes of YOFA due to the junction of asperities that form as a result of the stick-slip situation. Additionally, if YOFA wear debris remains entrapped across the sliding rubbing interface, it can cause aggravated abrasive actions due to the third-body mechanism. The secondary layer can also fragment due to the rubbing of soft wear debris from the matrix phase. With increasing YOFA particle size, all of these mechanisms become stronger, leading to further debonding and dislodging of material exposed from the primary surfaces.

3) Effect of Normal Load on Wear Test

The composite specimens' wear rate and loss gradually increase with the applied normal load, regardless of composition or other factors. When a specimen is mounted, its surface asperities come into contact with the counter asperities on the disc surface. As a normal load is applied, the asperities undergo elastic deformation before plastic deformation occurs. This process forms weak junctions through atomic diffusion, resulting in a stick-slip phenomenon. The junction fractures as the disc moves, generating ceramic wear debris. This cycle of junction formation, deformation (elastic/plastic), fracturing, and reformation continues, generating wear volumes. When two surfaces rub against each other, small particles can break off and cause wear. These particles can either leave the rubbing area or become stuck, leading to increased wear and faster deterioration. Soft debris from the surface can also be added to this wear, forming a secondary layer that breaks down over time. When more load is applied to the rubbing surfaces, they become stronger due to increased plastic deformation and atomic diffusion. Thus, increased stress is necessary to fracture the material, which reduces wear volumes under increasing loads. Additionally, interfacial heat generation at the asperity junction increases with increasing load, leading to partial melting of the matrix. This melted material spreads over the surfaces and promotes adhesive wear that counteracts the effects of abrasive wear. Additionally, Archard's law, as shown in Eq. (7), states that wear loss increases with the applied loads due to the rise in compressive and frictional forces. As the applied loads increase, the amount of frictional heat generated between the tribosurfaces also increases, which in turn reduces the resistance of the matrix composite to deformation, shear force, and detachment of the reinforcement particles from the composite surface. Moreover, increasing normal loads can cause progressive material removal, in which the material gets worn away from the composite surface, exposing weaker regions or delaminating the composite, further accelerating wear. A similar trend was observed by Alshabander et al. [15] and Ramanjaneyulu et al. [42], who found that the wear rate increased significantly with the increase in the applied normal load in RHDPE/CFA and HDPE/oxide composites, respectively.

4) Effect of Sliding Time on Wear Test

The wear rates significantly declined, whereas wear loss was considerably increased with increasing sliding time, which means sliding distance for all other factors. The considerable reduction in wear rate with increased sliding time, irrespective of composition, can be attributed to several factors, including the multipass condition, where repeated passes cause a decrease in abrasive severity and result in minimum wear for the maximum test duration. Furthermore, the main reason for the reduction in wear rate with increasing sliding distance can be attributed to the phenomenon known as "running-in" or "mating" of the sliding surfaces. In the initial stages and beginning of the sliding process, the surfaces of composite materials are rough and have bumps or unevenness. As the sliding continues, these bumps become flattened or worn down due to plastic deformation, thereby increasing the contact area between the sliding surfaces and reducing the pressure or stress concentration in that area. Reducing stress concentration is crucial in minimizing wear, as high local pressures can result in material removal and surface damage. By decreasing stress concentration, composite materials can distribute the applied load over a larger surface area, thus reducing the severity of

wear. As the sliding distance increases, composite materials can undergo a process known as "self-mating." During initial sliding, worn particles can become embedded or dispersed within the sliding interface. These particles act as solid lubricants or fillers and form a boundary layer between the sliding surfaces, especially the YOFA particles, with a high content of sulfur, sulfites, and TOC, as well as other materials, as shown in Table 1. This boundary layer can provide lubrication, reducing direct surface-to-surface contact and thereby further reducing wear. As the sliding distance increases, composite materials tend to adapt to specific sliding conditions, including temperature, humidity, and lubrication. This adaptation can change the material's microstructure, surface chemistry, or mechanical properties. The material's response to sliding conditions can influence its wear behavior, and in some cases, this can result in a decrease in the wear rate over time. Additionally, when two surfaces rub against each other, they undergo a process known as the stick-slip mechanism. This mechanism initially leads to the formation of junctions between asperities that break when the surfaces move, resulting in the generation of wear debris. As the rubbing continues, the cycle of junction formation, deformation (elastic/plastic), fracturing, and reformation continues, creating more wear debris. These particles can be made of ceramic, metals, and sulfites; sometimes, they get released from the rubbing interface. If they remain entrapped, they can accelerate the wear rate of the surfaces via third-body abrasive action. As the sliding distance increases, the heat generated at the junctions between asperities increases, causing more matrix phases to melt and spread over the surfaces, minimizing the wear rate as adhesive wear continues to counterbalance the abrasive wear action. The soft wear debris from the matrix forms a secondary layer over the surfaces, which eventually fragments and adds to the wear volume. Chand et al. [40] found similar results when studying the HDPE/coal FA composites. They discovered that the wear rate decreases as the sliding distance increases, but it increases linearly with the concentration of coal FA.

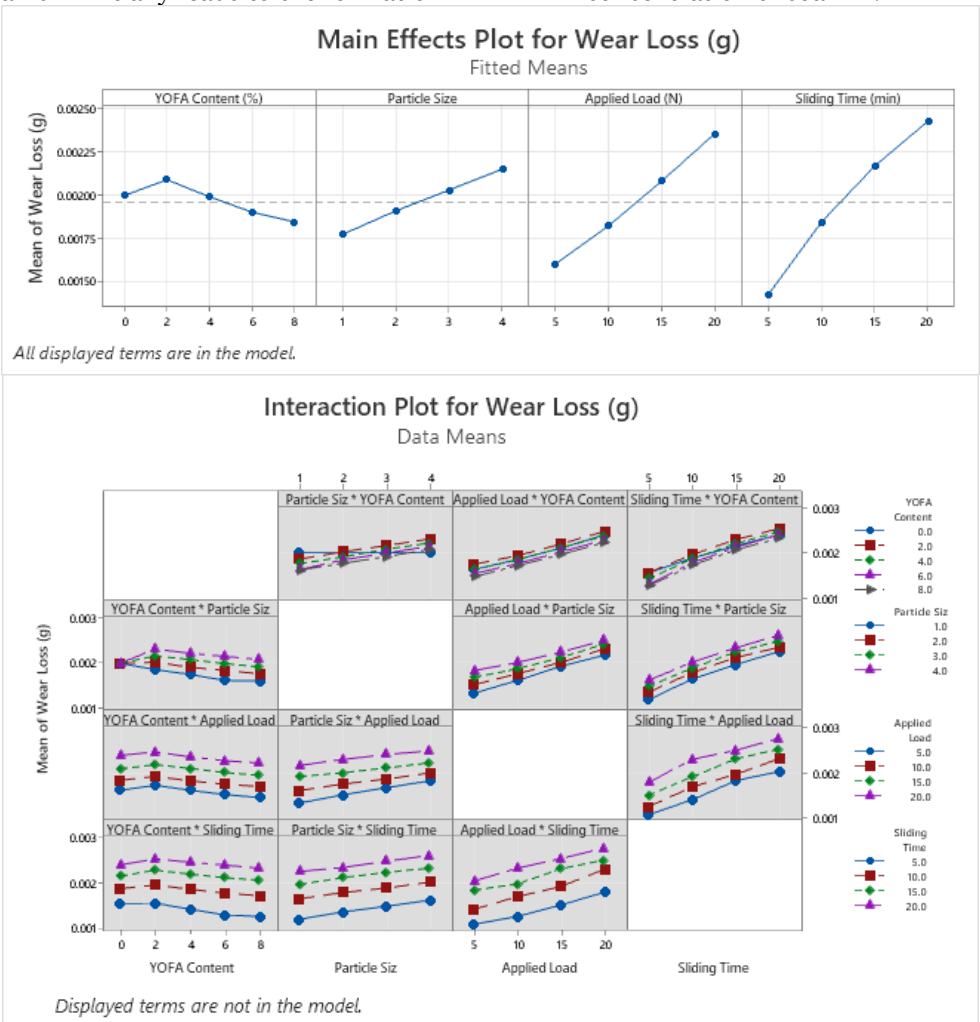

Fig. 9 Main and Interaction Effects Plots for Wear Loss in HDPE/YOFA Composites under Different Wear Factors.

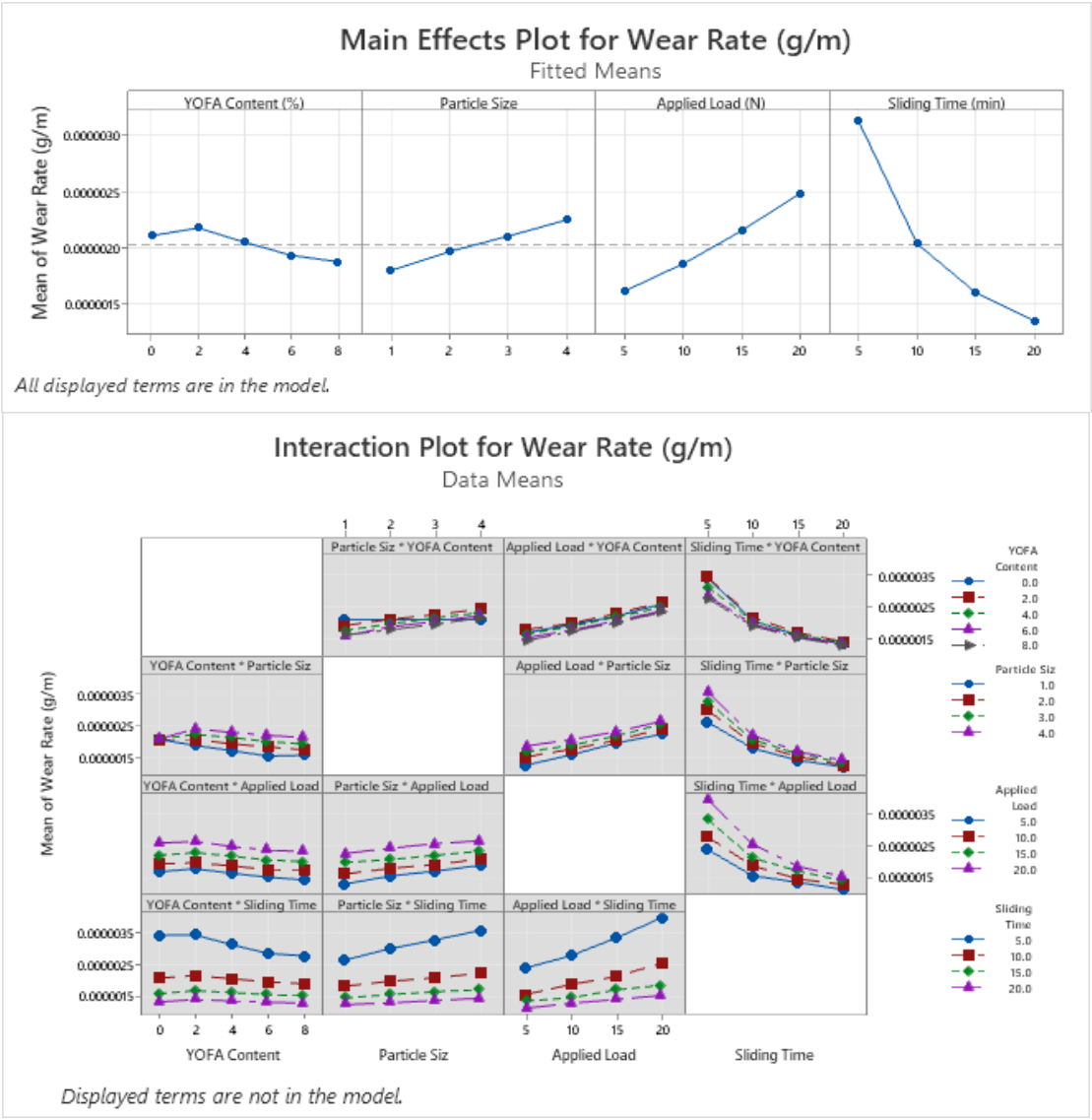

Fig. 10 Main and Interaction Effects Plots for Wear Rates in HDPE/YOFA Composites under Different Wear Factors.

3.4.2.Experimental design results

This study analyzed the impact of individual and combined operating factors on the wear loss and wear rate of HDPE/YOFA composites through FFD, ANOVA, and the Taguchi method in a steady-state environment.

3.4.2.1.Taguchi Method

Figure 11 displays the main effects plots for means and S/N ratios on both wear loss and wear rate, whereas Table 6 shows the ranking order of input parameters based on their significance. The MINITAB statistical software was used to determine the calculated/predicted S/N ratio for any parameter combination. It is worth noting that the mean S/N for wear loss and wear rate were 54.5 dB and 114.5 dB, respectively. The S/N ratio of wear loss and wear rate optimal parameter combinations is 56.0775 dB and 116.125 dB, respectively, for A5 B1 C1 D1 (8%, YOFA 1, 5 N, 5 min) and A5 B1 C1 D4 (8%, YOFA 1, 5 N, 20 min), which gives the ideal combination and should be chosen for the lowest wear condition, as shown in Table 6. A confirmational test must be conducted to verify the accuracy of the abovementioned findings. The data correlated to the confirmatory test of optimal process factors is presented in Additionally, a confirmation test should be performed for the chosen parameter combinations. The S/N ratio for wear loss and wear rate was predicted to be 60.8206 dB and 121.063 dB, respectively. The experimental results showed a measured S/N ratio of 56.0775 dB and 116.125 dB for the same parameter combination. The percentage errors for wear loss and wear rate were 7.798% and 4.078%, respectively, as indicated in Table 7. These results demonstrate that Taguchi's model or method is suitable for parameter optimization, with errors of 7.798% and 4.078%, making it a valuable tool for such studies. Furthermore, Table 6 shows the ranking order of the influence of significant factors: sliding Time, applied load, particle size, and YOFA content, respectively.

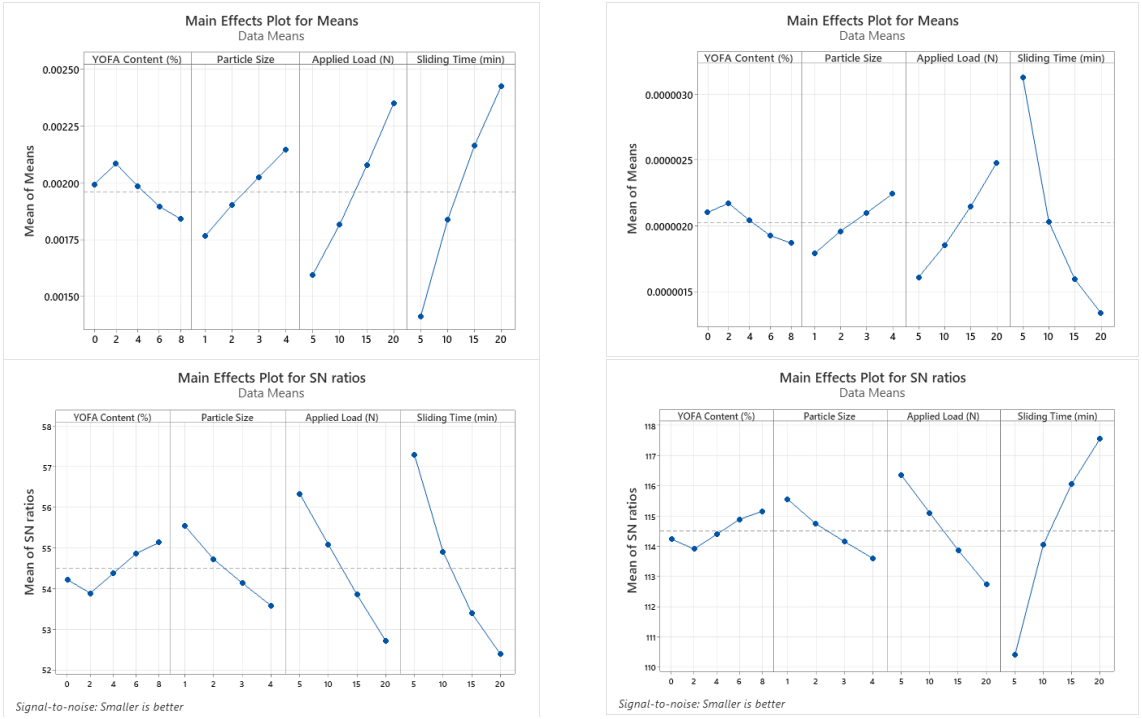

(A) (B)

Fig. 11 Main Effects Plots for Means and S/N Ratios of Input Control Factors on (A) Wear Loss and (B) Wear Rate.

Table 6 Ranking Order of Input Control Factors of Significance for (A) Wear Loss and (B) Wear Rate.

(A)

Level	A: YOFA Content (%)	B: Particle Size	C: Applied Load (N)	D: Sliding Time (min)
Response Table for Means.				
1	0.001994	0.001766	0.001596	0.001415
2	0.002084	0.001904	0.001818	0.001837
3	0.001986	0.002025	0.002076	0.002164
4	0.001897	0.002146	0.002351	0.002425
5	0.001841	-	-	-
Delta	0.000244	0.000380	0.000755	0.001010
Rank	4	3	2	1
Response Table for S/N Ratios (Smaller is better).				
1	54.22	55.54	56.34	57.30
2	53.89	54.72	55.09	54.91
3	54.37	54.14	53.85	53.40
4	54.87	53.58	52.71	52.39
5	55.13	-	-	-
Delta	1.25	1.96	3.62	4.91
Rank	4	3	2	1

(B)

Level	A: YOFA Content (%)	B: Particle Size	C: Applied Load (N)	D: Sliding Time (min)
Response Table for Means.				
1	0.000002	0.000002	0.000002	0.000003
2	0.000002	0.000002	0.000002	0.000002
3	0.000002	0.000002	0.000002	0.000002
4	0.000002	0.000002	0.000002	0.000001
5	0.000002	-	-	-
Delta	0.000000	0.000000	0.000001	0.000002
Rank	4	3	2	1
Response Table for S/N Ratios (Smaller is better).				
1	114.2	115.6	116.3	110.4
2	113.9	114.7	115.1	114.0
3	114.4	114.1	113.9	116.0
4	114.9	113.6	112.7	117.5
5	115.1	-	-	-
Delta	1.2	2.0	3.6	7.1
Rank	4	3	2	1

Table 7 Results of the Predicted and Experimental Confirmation for (A) Wear Loss and (B) Wear Rate.

		Optimal process factors	Predicted (dB)	Experimental (dB)	Error (%)
(A)	S/N ratio of wear loss.	A5 B1 C1 D1	60.8206	56.0775	7.798
(B)	S/N ratio of wear rate.	A5 B1 C1 D4	121.063	116.125	4.078

3.4.2.2.FFD of the Experiment

ANOVA is a statistical methodology used to separate the individual effects of all control factors. Furthermore, ANOVA is a numerical design procedure that breaks down the specific effects of all control factors. It measures the percentage contribution of each control factor to determine its corresponding effect on the quality characteristic [45, 46]. Tables 8 and 9 present the summary of the results of the ANOVA analysis, with a significance level (P-value) of 0.05, indicating a 95% confidence level. In these Tables, the values in column 5 represent "Adj SS," which stands for Adjusted Sum of Squares, measuring the fraction of variability in the dependent variable that is explained by changes in the independent variables. A statistical test, such as an F-statistic in the ANOVA case, is crucial in determining whether the test is significant. The F-statistic follows an F-distribution under the null hypothesis. The "F_0 value" is the ratio of the variance of the factor mean square divided by the variance of the error mean square. The P-value represents the probability that the test statistic takes on a value as extreme as, or more

extreme than, the observed value of the statistic when the null hypothesis H_0 is true [46]. All the probability values (P values) and the error contribution of the composite preforms are approximately zero, indicating that the factors are significant and greatly influence the wear loss and wear rate. The degrees of freedom "DF" indicate the contribution of controllable factors [46]. The ANOVA table indicates that the error sum of squares remains zero, suggesting that only one replication was considered in the experiment design, which involved four factors: composition, particle size, applied load, and sliding time, as well as two responses: wear loss and wear rate. Because only one replication was considered for wear loss and wear rate, the degrees of freedom remain at zero. Consequently, the error sum of squares and the error mean sum of squares also remain at zero. As a result, the F_0 value column remains at zero. The R-squared statistic indicates that the model closely describes 99.82% and 99.85% of the variability in wear loss and wear rate, respectively. The adjusted R-squared statistics are 99.48% and 99.55%, and the predicted R-squared values account for 98.46% and 98.66% of the variability in the same two response sequences. The coefficient of determination (R-squared) reflects how well the model fits the data. In this case, the high determination coefficient value indicates the strong significance of the developed model [47]. The ANOVA table indicates no residual error, meaning that the control parameters selected in the study and their interactions have statistical and physical significance in the wear loss and wear rate of the composites, with the percentage contribution of their interactions being greater than the error. Furthermore, the fourth column of the tables (contribution) indicates the parameters that have a greater impact on controlling or monitoring the output response. The contribution column found that the main factors influencing wear loss and wear rate were sliding time (D) and the applied load (C). The remaining factors, YOFA content (A) and particle size (B), as well as the 2-way and 3-way interaction effects, had a relatively small influence. Notably, the sliding time and applied load obtained for the composite preforms are the primary factors controlling the wear loss and wear rate of the composites, surpassing other factors and interactions. Additionally, the interaction effects of the preforms on wear loss and wear rate are marginal compared to their individual effects. The 4-way interaction effect was rejected at a 95% confidence level, indicating a small residual error. The response values are influenced not only by the control factors A, B, C, and D, which are considered in this study, but also by experimental irregularities (uncontrollable or noise factors), such as environmental conditions, machine vibrations, and the surface finish of both the pin and the disc. The tribological behavior of polymers and polymer composites is closely linked to their viscoelastic and temperature-related properties. When two materials come into sliding contact, heat is generated at the contact points, leading to an increase in interface temperature. This rise in temperature affects the viscoelastic properties, influencing the material's stress response, adhesion, and transfer behaviors. Prolonged sliding time further elevates the friction surface temperature, which can significantly degrade the mechanical properties of the composites and lead to material loss [45]. Therefore, sliding time and applied load are key factors in determining wear characteristics, surpassing other factors and interactions. Figure 12 shows the Pareto chart that displays the effects of wear loss, whereas the Pareto chart for wear rates is not displayed because the standard error for effects is zero. The Pareto plot visually represents the main factors and their interactions, showing their absolute values. The reference line serves as a marker to indicate parameters with a relatively higher degree of importance that extend beyond it. As shown in Fig. 12, the factors with the least influence on wear loss are ABD and AC, which have P values of 0.183 and 0.137, respectively. Furthermore, other factors and interactions significantly impact wear behavior.

Table 8 ANOVA Results for Wear Loss (Neglecting 4-Way Interaction Effects).

Source	DF	Seq SS	Contribution (%)	Adj SS	Adj MS	F-Value	P-Value
Model	211	0.000083	99.82	0.000083	0.000000	291.33	0.000
Linear	13	0.000080	95.81	0.000080	0.000006	4538.55	0.000
A: YOFA Content (%)	4	0.000002	2.73	0.000002	0.000001	420.35	0.000
B: Particle Size	3	0.000006	7.65	0.000006	0.000002	1570.52	0.000
C: Applied Load (N)	3	0.000026	30.68	0.000026	0.000009	6296.76	0.000
D: Sliding Time (min)	3	0.000046	54.76	0.000046	0.000015	11239.30	0.000
2-Way Interactions	63	0.000003	3.40	0.000003	0.000000	33.23	0.000
A×B	12	0.000002	1.96	0.000002	0.000000	100.82	0.000
A×C	12	0.000000	0.03	0.000000	0.000000	1.49	0.137
A×D	12	0.000000	0.47	0.000000	0.000000	24.24	0.000
B×C	9	0.000000	0.31	0.000000	0.000000	20.98	0.000
B×D	9	0.000000	0.08	0.000000	0.000000	5.30	0.000
C×D	9	0.000000	0.55	0.000000	0.000000	37.56	0.000
3-Way Interactions	135	0.000001	0.61	0.000001	0.000000	2.79	0.000
A×B×C	36	0.000000	0.16	0.000000	0.000000	2.76	0.000

A×B×D	36	0.000000	0.07	0.000000	0.000000	1.26	0.183
A×C×D	36	0.000000	0.21	0.000000	0.000000	3.54	0.000
B×C×D	27	0.000000	0.17	0.000000	0.000000	3.87	0.000
Error	108	0.000000	0.18	0.000000	0.000000		
Total	319	0.000083	100.00				

where DF = Degrees of Freedom; Seq SS = Sequential Sums of Squares; Adj SS = Adjusted Sum of Squares; Adj MS = Adjusted Mean of Squares.

Model Summary:

S	R-sq	R-sq(adj)	PRESS	R-sq(pred)	AICc	BIC
0.0000368	99.82%	99.48%	0.0000013	98.46%	-4688.40	-4745.78

Table 9 ANOVA Results for Wear Rate (Neglecting 4-Way Interaction Effects).

Source	DF	Seq SS	Contribution (%)	Adj SS	Adj MS	F-Value	P-Value
Model	211	0.000000	99.85	0.000000	0.000000	335.68	0.000
Linear	13	0.000000	89.86	0.000000	0.000000	4903.22	0.000
A: YOFA Content (%)	4	0.000000	1.80	0.000000	0.000000	319.62	0.000
B: Particle Size	3	0.000000	4.13	0.000000	0.000000	976.00	0.000
C: Applied Load (N)	3	0.000000	15.47	0.000000	0.000000	3657.56	0.000
D: Sliding Time (min)	3	0.000000	68.46	0.000000	0.000000	16187.55	0.000
2-Way Interactions	63	0.000000	9.01	0.000000	0.000000	101.43	0.000
A×B	12	0.000000	1.08	0.000000	0.000000	64.08	0.000
A×C	12	0.000000	0.04	0.000000	0.000000	2.20	0.016
A×D	12	0.000000	1.47	0.000000	0.000000	86.77	0.000
B×C	9	0.000000	0.17	0.000000	0.000000	13.59	0.000
B×D	9	0.000000	1.67	0.000000	0.000000	131.71	0.000
C×D	9	0.000000	4.58	0.000000	0.000000	360.67	0.000
3-Way Interactions	135	0.000000	0.98	0.000000	0.000000	5.16	0.000
A×B×C	36	0.000000	0.11	0.000000	0.000000	2.16	0.001
A×B×D	36	0.000000	0.51	0.000000	0.000000	10.02	0.000
A×C×D	36	0.000000	0.18	0.000000	0.000000	3.57	0.000
B×C×D	27	0.000000	0.18	0.000000	0.000000	4.80	0.000
Error	108	0.000000	0.15	0.000000	0.000000		
Total	319	0.000000	100.00				

where DF = Degrees of Freedom; Seq SS = Sequential Sums of Squares; Adj SS = Adjusted Sum of Squares; Adj MS = Adjusted Mean of Squares.

Model Summary:

S	R-sq	R-sq(adj)	PRESS	R-sq(pred)	AICc	BIC
0.0000001	99.85%	99.55%	0.0000000	98.66%	-8845.65	-8903.04

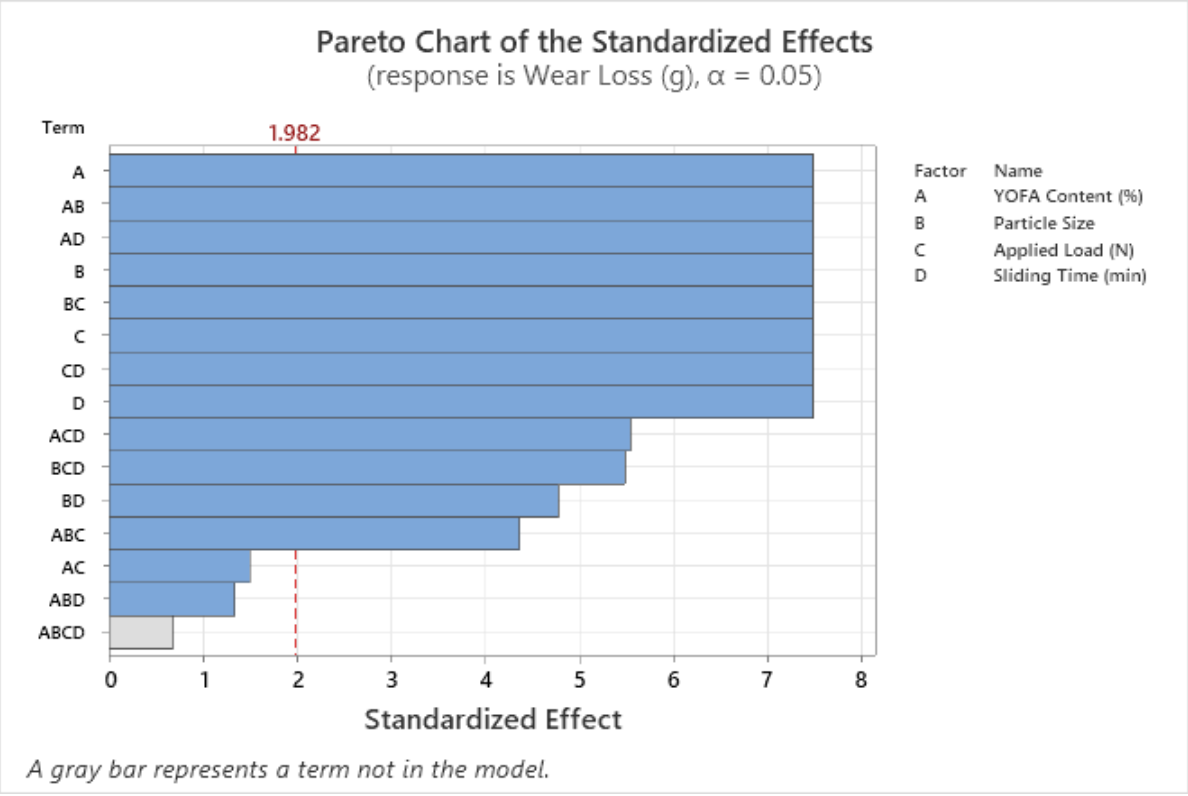

Fig. 12 Pareto Chart of the Factors Affecting Wear Loss.

3.4.2.2.1.Interpretation of Residual Graphs

A normal probability plot (NPP) of the residuals was created to verify the normality of the data. Residuals represent the variation between the experimental and predicted values from the linear regression [46,47]. Figures 13(a) and 14(a) display the NPP for the wear loss and wear rate of HDPE/YOFA composites, respectively. These probability plots clearly show that the observed values are very close to the normal (straight) probability line, indicating that the errors are negligible and the model is adequate. The histogram shows the distribution of residuals for all interpretations (320 runs). Figures 13(b) and 14(b) indicate an almost bell-shaped symmetrical histogram. Figures 13(c) and 14(c) depict the residuals versus the fitted values (predicted response) for wear loss and wear rate. The scatter of the residuals is random, about zero, implying that the errors are negligible and have constant variance. When using a line sequence to collect the data, the order of the runs affects the responses. Figures 13(d) and 14(d) show the plots of the residual value and the order of the corresponding experimental measurements. The results (responses) are influenced by the order of the observations (runs) in a design where the runs are regular. This plot is particularly useful for a developed design with regular runs.

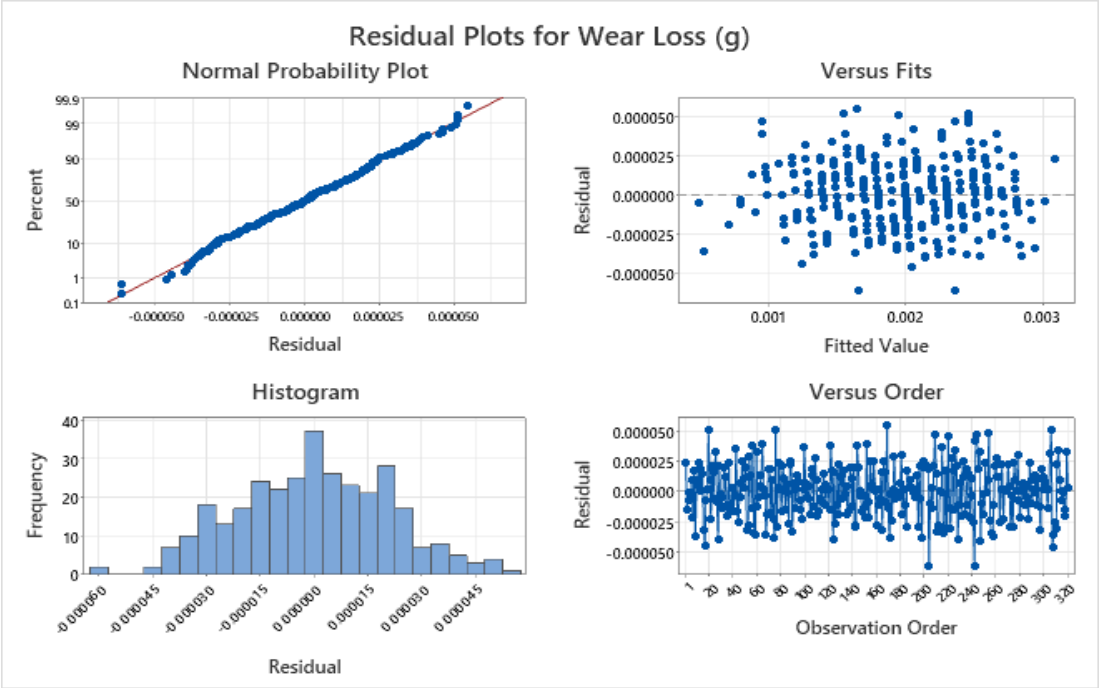

Fig. 13 Residual Plots for Wear Loss.

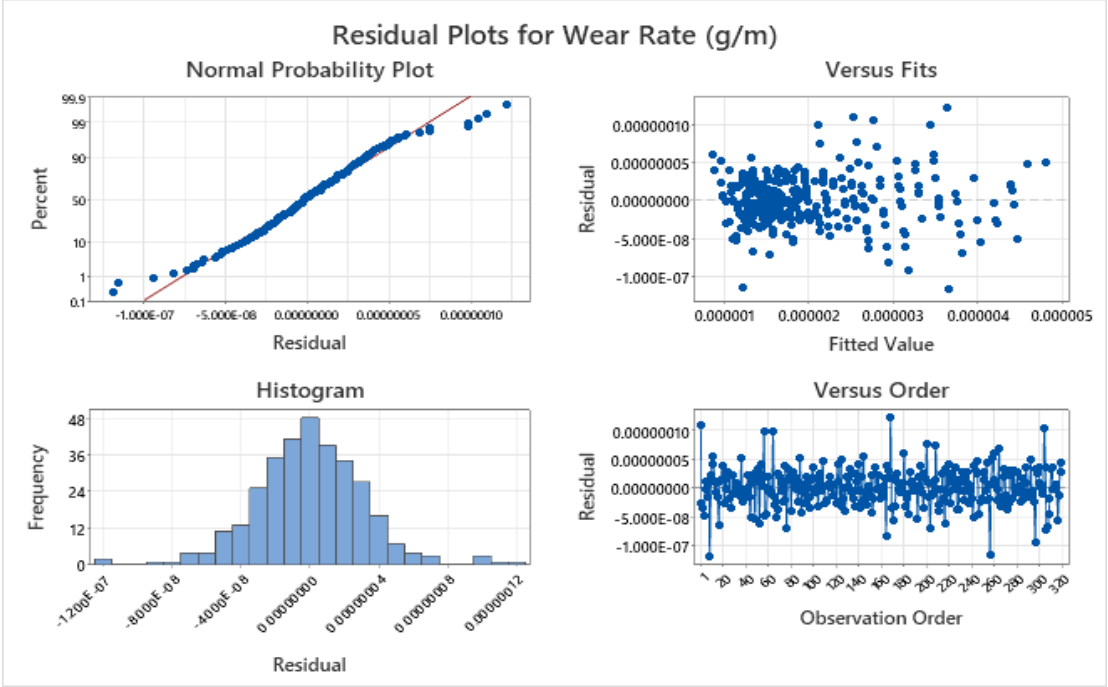

Fig. 14 Residual Plots for Wear Rate.

3.4.3.Morphology Analysis of Wear Surface

The wear characteristics of the HDPE/YOFA composites are subject to monitoring and control through the operational parameters of dry sliding wear, specifically sliding time, applied load, particle size, and YOFA content, in sequential order. These parameters, along with their respective levels or values, as tabulated in Table 5, were observed through parametric optimization using both Taguchi's method and the full factorial design of the experiment. The abrasive wear behavior exhibited by polymers and their composites is a complex phenomenon that remains inadequately understood. The literature offers limited information and presents divergent viewpoints on the abrasive wear performance of particle-reinforced composites. Generally, the wear properties of particle-reinforced composites depend on various parameters, including toughness, stiffness, hardness, component concentrations, and particle-matrix adhesion. Since abrasive wear entails tearing away materials, the pivotal role of strength and hardness in determining the wear properties of particle-reinforced polymer composites cannot be overstated. Notably, the test results and SEM observations provide the basis for several pertinent observations [33, 35]. The wear rate significantly affects the surface morphology of the tested sample as well as the type and size of wear debris. During the initial sliding period, the steel disc will deform the surface and remove particles from the relatively softer composite material as the softer material slides over the hard material (the steel disc). These particles, known as wear debris, will fill the wear valleys and become stuck on both the disc and sample surfaces, causing the friction mode to change from adhesion to abrasion. This conversion leads to the machining of the sample surface. Polymers and their composites exhibit viscoelastic properties, and their deformations under load are also viscoelastic in nature. When a steel disc moves over a soft polymer surface, it causes a plowing action that increases the severity of abrasive wear, especially when ground with grade 1000 emery paper. Additionally, the wear resistance of thermoplastics cannot be improved by incorporating coarse particles when the wear mechanism is highly abrasive. Due to these reasons, it is believed that the abrasive wear behavior of the composites deteriorates compared to neat HDPE. Analyzing the surface morphology of worn-out surfaces is crucial for understanding the predominant wear mechanism or sub-mechanism responsible for surface damage during sliding. Figure 15 presents the micrographs of the damaged surface under steady-state conditions. The damaged surface morphology of (A2 B4 C4 D1) (2 wt.%, YOFA 4, 20N, and 5 min) was scrutinized due to its maximum wear rate. Upon examining the micrograph, it is evident that the wear mechanism is causing a high wear rate in the composite specimens. Severe wear has led to the exposure of the primary surface and reinforcing phases, such as particulate pull-out. Additionally, a significant amount of wear debris is dispersed randomly over the surface, some of which remains entrapped across the rubbing interface. Due to their ceramic nature, these wear debris can accelerate wear rates through a third-body abrasive mechanism. Sometimes, they form a secondary or subsurface layer by being laminated over the primary surfaces and loosely held in place over them. The delamination or fragmentation of such a layer would be attributed to the plowing action of other wear particles, including third-body or abrasive particles, or the ceramic nature of the wear particles during the sliding action. This phenomenon would further contribute to wear volumes. Visible surface cracking and micro-cracks in many areas would lead to dislodging the reinforcing phases and subsequently result in micro-pit formation. When the pin contacts the disc surface under a low applied normal load, the asperities at the junction touch and deform elastically, undergoing plastic straining, which leads to the welding of the junctions. Atomic diffusion across asperities would also contribute to this process [33, 48]. In a stick-slip situation, as the pin starts moving, the formed junction fractures, generating a significant amount of wear debris and causing the reinforcing phases to become dislodged and exposed, leading to micro-cracking of the surface at multiple sites, resulting in the formation of micro-pits. In contrast, the micrograph in Fig. 16 illustrates the optimal minimization of wear rate severity under wear conditions (A5 B1 C1 D4) (8 wt.%, YOFA 1, 5 N, 20 min). Abrasion occurs when a harder material is removed from a softer one, resulting in debris at the interface or on the harder surface. The presence of wear debris can enhance the wear resistance of composites through a favorable rolling effect. Moreover, certain fillers and their debris, such as TOC, sulfur, and sulfites, can diminish friction by serving as a solid lubricant. Therefore, a comprehensive examination of these debris formations at the interface or their entrapment on the harder surface is essential for a thorough understanding of the abrasive wear characteristics of tribo-pairs. This study revealed that most of the wear debris adhered to the surface of the steel disc, thereby promoting two-body abrasive wear. As the sliding time increases, junction strength is further reinforced due to significant atom diffusion across the asperities contact or extensive plastic deformation. This behavior results in a heightened stress requirement for fracture. The heightened heat generated during

rubbing or junction rupturing leads to partial matrix melting, which spreads over the primary surface and becomes reinforced; consequently, the intensity of abrasive wear is reduced as adhesive wear takes precedence. This mechanism is further strengthened under lower loads, where adhesive wear supersedes abrasive wear. Additionally, the micrograph suggests a less abrasive action, which is offset by adhesive wear as the sliding distance increases. With increased rubbing distance, heat generation and accumulation across the rubbing surfaces would cause partial melting of the matrix phases, promoting adhesive wear over abrasive wear, reducing wear rates. There is less plowing or grooving action, surface cracking, pitting, and wear debris visible on the surfaces. The primary surfaces appear intact, with less exposure to ingredients, and the secondary layers exhibit less fragmentation, resulting in lower wear debris and wear volumes for the composite specimens being studied.

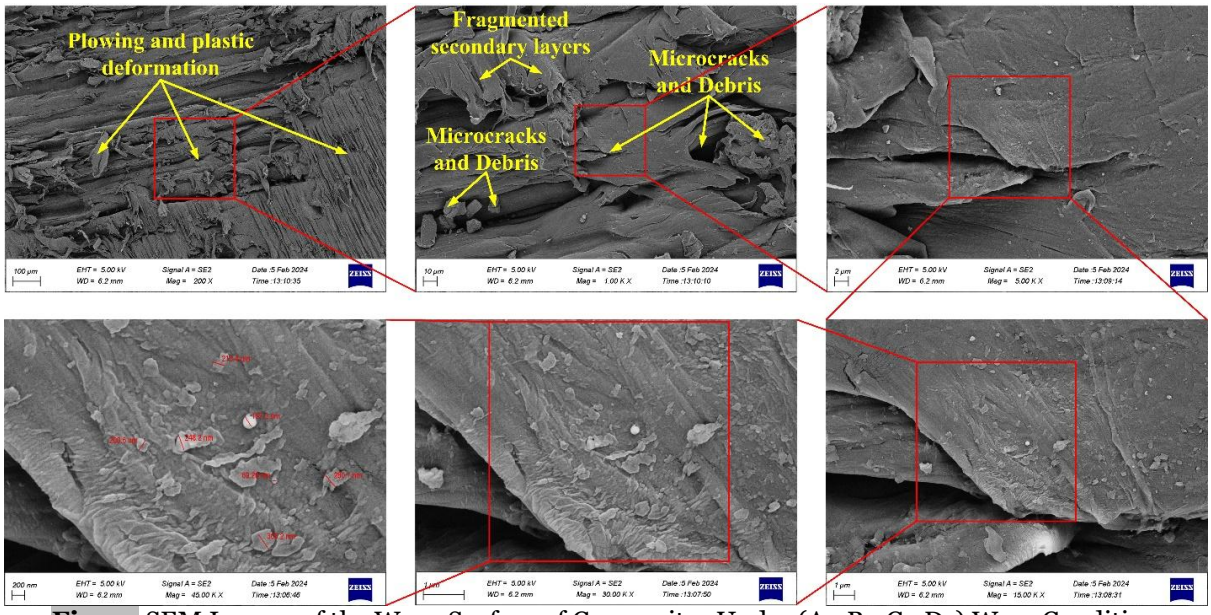

Fig. 15 SEM Images of the Worn Surface of Composites Under (A2 B4 C4 D1) Wear Condition Factors.

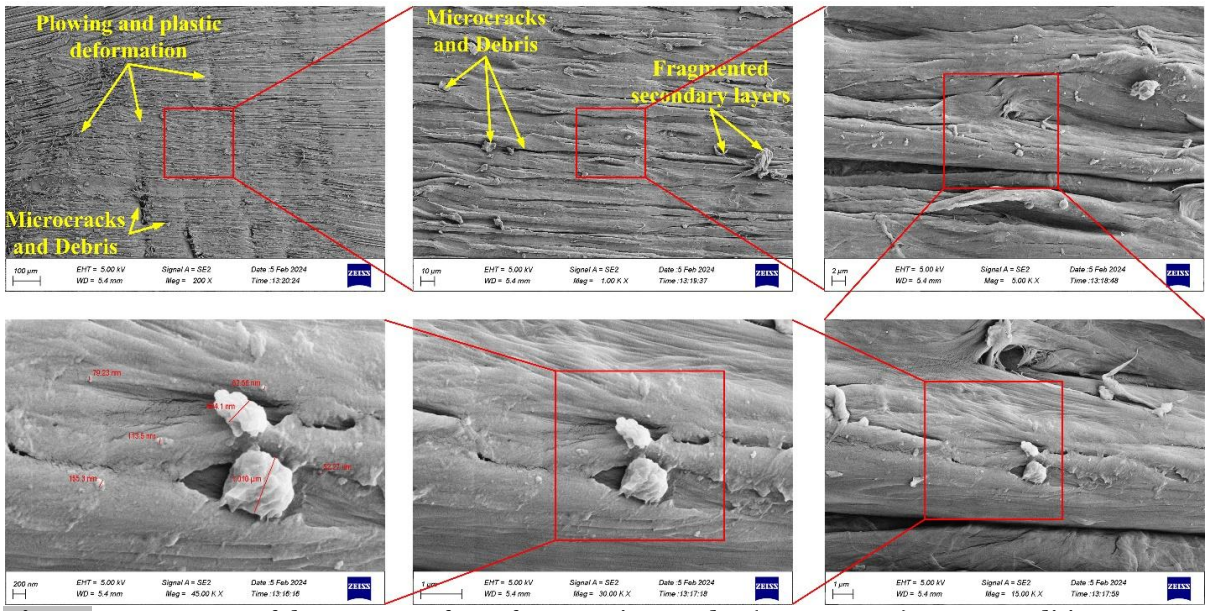

Fig. 16 SEM Images of the Worn Surface of Composites Under (A5 B1 C1 D4) Wear Condition Factors.

With increased applied loads, Fig. 17 demonstrates that the composites for wear conditions (A4 B3 C3 D3) (6 wt.%, YOFA 3, 15 N, and 15 min) gradually deteriorate due to the development of shear stress by the hard surface, resulting in increased ditches and debris loss. This Figure shows wear mechanisms causing significant wear on the composite specimens. Deep plowing/grooving marks have dislodged materials from the surface at many sites, exposing the reinforcing phases to the environment. The broken or dislodged reinforcing phases act as ceramic wear debris, accelerating abrasive wear when they become entrapped across the rubbing interface or remain in contact with it. This

intense abrasive action can lead to surface cracking at many sites, resulting in pit formation and increased wear volumes. The rubbing of wear debris against the primary surface leads to the formation of a secondary layer of debris. This loosely held layer contributes to increased wear volumes as it fragments during the sliding process. Additionally, the intense elastic-plastic deformation of boundaries and atomic diffusion caused by heating at the initial stage lead to the formation of stick-slip junctions across surface asperities. These junctions fracture as soon as the disc starts to move for shorter distances. At higher applied loads, the intensity of pits and ditches is greater compared to lower applied loads. Additionally, plastic deformation of the ditch boundary material occurs, generating more frictional heat between the contact surfaces. The continuous application of high loads over time leads to delamination, cracking, and shear forces on the sample surface, causing the development and advancement of digs toward the edges of the ditches. Additionally, the softer matrix material is dug by the harder counter steel disc, resulting in the formation of cracks that spread laterally and axially, deforming the subsurface of the sample. Furthermore, the appearance of digs, ditches, and texture along the matrix material surface is uniform across all worn surfaces, indicating the distribution of material lumps due to the high ductility properties of the material matrix. Upon visual inspection of the worn surface, it is evident that wear loss is attributed to delamination and micro-cutting (abrasion wear). The size and shape of wear debris are significantly influenced by the applied loads. Under low applied loads, the wear debris exhibits a shiny, less bright coloration and uniform, small size. Conversely, high-applied loads result in the production of larger, irregularly shaped debris with a grey color. Moreover, the wear rate intensifies under high loads, generating debris with a texture similar to that of the tested sample. The texture of debris produced from the composite material differs from that of the matrix material, and intermittent dark oxidation regions are observed along the worn surface of the composite.

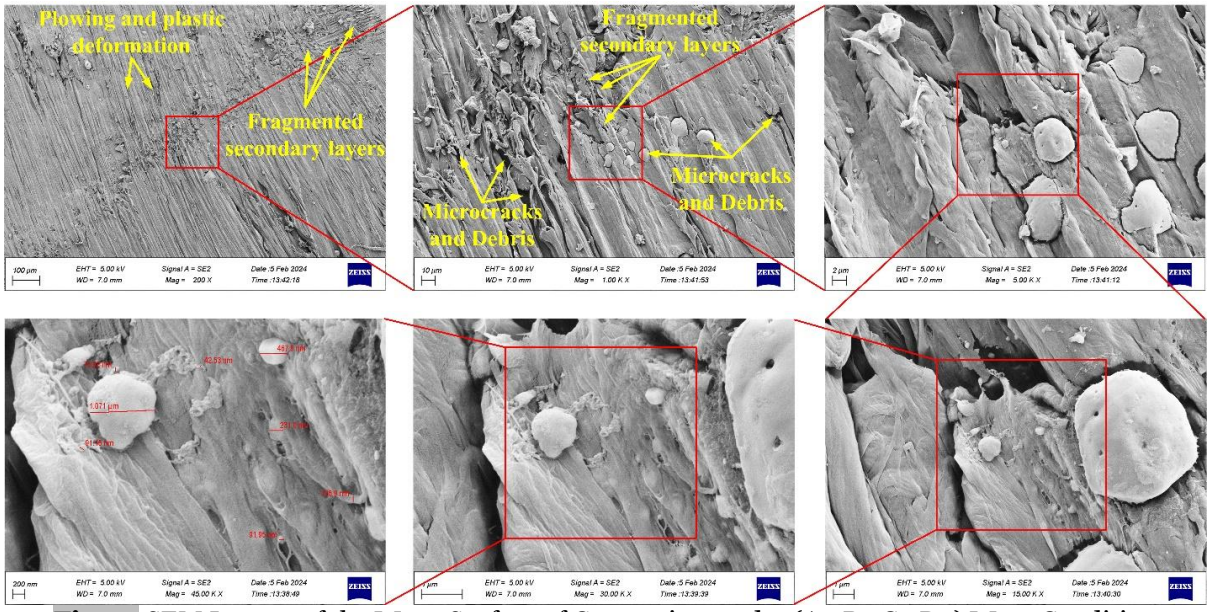

Fig. 17 SEM Images of the Worn Surface of Composites under (A4 B3 C3 D3) Wear Condition Factors.

The SEM images in Fig.18 show the worn surfaces of the samples under the following wear conditions: (A3 B2 C2 D2) (4 wt.%, YOFA 2, 10N, and 10 min). The worn surface is rougher than the unworn side due to microplowing and microcutting features resulting from dry sliding wear. These mechanisms were always accompanied by plastic deformation in all the composites tested. During the wear test, it was observed that the filler particles within the matrix did not protrude on the worn surface of the samples, as the matrix enveloped the particles due to plastic deformation. Generally, adhesion, abrasion, and fatigue are noted as the predominant wear modes in polymers. In contrast, the samples did not show signs of fatigue wave or crack formation due to the cyclic pass of an asperity of the counterpart on the surface. This behavior is believed to be linked to the increased plastic deformation and abrasive nature of the steel disc. Furthermore, in the two-body abrasive wear process, the actual contact area between the composite surface and the abrasive particles decreases with larger particle sizes, leading to higher stress levels at the contact surface of the tribepairs, which results in early crack initiation in the matrix and ultimately in high wear rates of the composite. In short, plowing and cutting mechanisms are the predominant types of wear

observed in all samples during abrasive wear. The particles from the trapped wear debris were found on the wear tracks of the samples and on the opposing steel disk. The trapped wear debris was also observed to create a continuous phase, particularly at the edge of the samples. This behavior is primarily caused by the lack of fillers near the surface of the samples, resulting from the injection molding process and the plastic deformation of the matrix material under the applied normal load. On the other hand, Fig.19 shows the SEM micrographs of the net HDPE at an applied load of 10 N and a sliding time of 10 min, respectively. This figure shows slightly less abrasive action, as adhesive action tends to counterbalance it. As a result, the secondary layers appear more intact and less fragmented, with fewer surface cracks, pits, and wear debris. The primary surface also seems relatively intact, with fewer exposed reinforcing phases. Therefore, the frequency of the mechanism intensifies the action, leading to a more severe wear rate for the composite being studied. With a greater sliding distance, the surfaces experience higher heat generation, potentially causing partial melting of the matrix phases that spread over the pin and disc surfaces, which would help reduce the severity of wear rates.

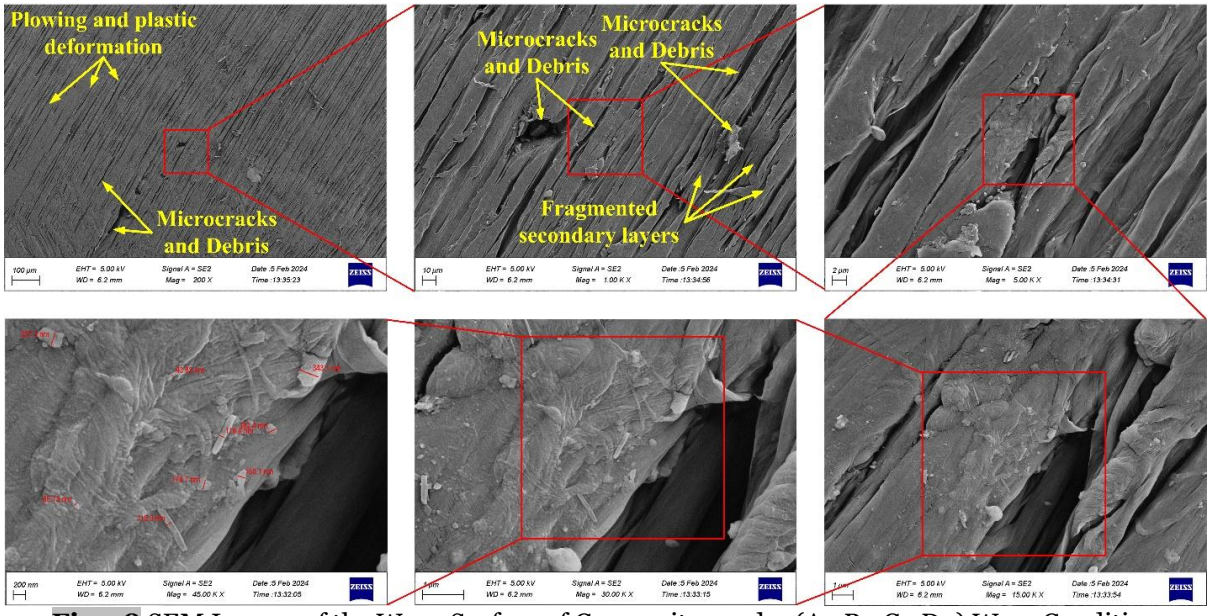

Fig. 18 SEM Images of the Worn Surface of Composites under (A3 B2 C2 D2) Wear Condition Factors.

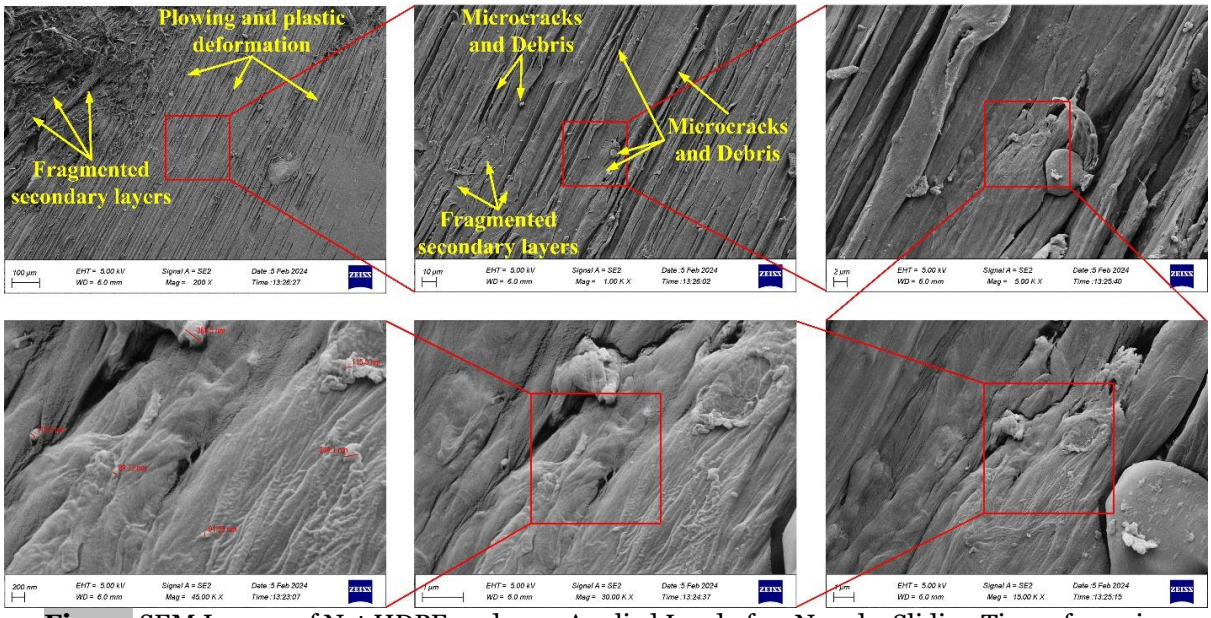

Fig. 19 SEM Images of Net HDPE under an Applied Load of 10 N and a Sliding Time of 10 min.

4.CONCLUSIONS

In the current study, high-density polyethylene (HDPE) was successfully reinforced with a new type of heavy fuel oil fly ash, known as yellow oil fly ash (YOFA), to prepare composites using the injection molding technique. The study investigated the impact of YOFA content and particle size on the physical, mechanical, and wear properties of HDPE/YOFA composites. Additionally, the study examined the effects of applied load and sliding time on the wear test. The main conclusions are summarized below:

1) Both the theoretical and experimental densities increased linearly with the YOFA content, while the experimental density slightly decreased with increasing particle size of YOFA. The theoretical density remains much higher than the experimental ones.

2) Void content, water absorption, and thickness swelling gradually increased with increasing both the concentration and particle size of YOFA particles.

3) Shore D hardness shows a reverse trend with void content, where hardness slightly decreases with increased YOFA content and particle size.

4) The FFD of the experiment and Taguchi approach reveals that sliding time, applied normal loads, YOFA particle size, and YOFA content are the significant contributors to wear factors, respectively. Such tools are extremely useful for optimizing parameters, assessing their order of significance, and designing experimental trials, with an error of 7.798% for wear loss and 4.078% for wear rate.

5) Under steady-state conditions, the wear resistance decreases with YOFA particle size and normal applied load and also declines with YOFA content up to 2 wt.%, followed by gradual improvement up to 8 wt.%. In contrast, with increasing sliding time, the wear loss considerably increases while the wear rate significantly improves.

6) The surface morphology analysis shows the mechanisms responsible for surface damage during sliding wear tests, including pit formation, cracking, lamination, plowing action, and delamination.

7) The optimal conditions for wear loss were a YOFA content of 8 wt.%, the smallest particle size, an applied load of 5 N, and a sliding time of 5 minutes. Conversely, the optimal conditions for the wear rate are the same as those for wear loss, except for the sliding time, which was 20 minutes.

REFERENCES

[1] Alghamdi MN. **Effect of Filler Particle Size on the Recyclability of Fly Ash Filled HDPE Composites.** *Polymers* 2021; **13**(16): 2836.

[2] Huang TY, Chiueh PT, Lo SL. **Life-Cycle Environmental and Cost Impacts of Reusing Fly Ash.** *Resources, Conservation and Recycling* 2017; **123**: 255–260.

[3] Ju S, Yoon J, Sung D, Pyo S. **Mechanical Properties of Coal Ash Particle-Reinforced Recycled Plastic-Based Composites for Sustainable Railway Sleepers.** *Polymers* 2020; **12**(10): 2287.

[4] Bakshi P, Pappu A, Patidar R, Gupta MK, Thakur VK. **Transforming Marble Waste into High-Performance, Water-Resistant, and Thermally Insulative Hybrid Polymer Composites for Environmental Sustainability.** *Polymers* 2020; **12**(8): 1781.

[5] Miller L, Soulliere K, Sawyer-Beaulieu S, Tseng S, Tam E. **Challenges and Alternatives to Plastics Recycling in the Automotive Sector.** *Materials* 2014; **7**(8): 5883–5902.

[6] Sharma RP, Kumar M, Kumar A. **Dry Sliding Wear and Mechanical Investigations on Flyash Particulates - Lapinus Fibre - Polyamide 66 Polymer Composites: Ranking Analysis Using Hybrid Analytic Hierarchy Process-R Method.** *Journal of Elastomers & Plastics* 2023; **55**(7): 1035–1076.

[7] Nguyen KQ, Mwiseneza C, Mohamed K, Cousin P, Robert M, Benmokrane B. **Long-Term Testing Methods for HDPE Pipe - Advantages and Disadvantages: A Review.** *Engineering Fracture Mechanics* 2021; **246**: 107629.

[8] Ghafel SA, Namer NSM, Ali AH. **Study the Mechanical Properties and Fatigue Effect of Multilayer Woven E-Glass/Epoxy Composite under Constant and Variable Loading.** *Tikrit Journal of Engineering Sciences* 2023; **30**(2): 21–30.

[9] Alghamdi MN. **Performance for Fly Ash Reinforced HDPE Composites over the Ageing of Material Components.** *Polymers* 2022; **14**(14): 2913.

[10] Chand N, Sharma P, Fahim M. **Abrasive Wear Behavior of LDPE Filled with Silane Treated Flyash Cenospheres.** *Composite Interfaces* 2011; **18**(7): 575–586.

[11] Omair N, Intan Syaqirah MZ. **Mechanical Properties of Recycled High-Density Polyethylene, Rice Husk Ash, and Fly Ash Composite Mixture.** *Journal of Innovation and Technology* 2022; **2022**(22): 1–8.

[12] Bash AM, Othman TT, Oleiwi JK. **Improving Mechanical Properties of Laminated Biocomposites for Artificial Lower Limb Socket.** *Tikrit*

Journal of Engineering Sciences 2023; **30**(3): 9–16.

[13] Sheykh MJ, Tarmian A, Doosthoseini K, Abdulkhani A. **Wear Resistance and Friction Coefficient of Nano-SiO2 and Ash-Filled HDPE/Lignocellulosic Fiber Composites.** *Polymer Bulletin* 2017; **74**(11): 4537–4547.

[14] Kareem Ibraheem T, Al-Taei AM. **Effect of Low-Density Polyethylene on the Stripping Properties under Fatigue Loading of Binder Layer of HMA Mixtures.** *Tikrit Journal of Engineering Sciences* 2021; **27**(4): 102–113.

[15] Alshabander BM, Mohammed AA, Khalil AS. **Mechanical Properties and Thermal Conductivity of Coal Ash-Recycled High-Density Polyethylene Composite.** *Journal of Molecular and Engineering Materials* 2018; **6**(1): 1850002.

[16] Mohammed QY, Taher SR. **Determination of Vanadium in Crude Oil and Some Petroleum Products Spectrophotometrically.** *Journal of Chemical and Pharmaceutical Sciences* 2018; **11**(1): 118–121.

[17] Mustafa AN, Ali OM, Alomar OR. **Effect of Heavy Fuel Combustion in a Gas Power Plant on Turbine Performance: A Review.** *International Journal of Design & Nature and Ecodynamics* 2022; **17**(1): 102–111.

[18] Salehnasab B, Poursaeidi E, Mortazavi SA, Farokhian GH. **Hot Corrosion Failure in the First Stage Nozzle of a Gas Turbine Engine.** *Engineering Failure Analysis* 2016; **60**: 316–325.

[19] Montero X, Galetz MC. **Coatings for Boiler Components Exposed to Vanadium-Containing Oil Ash in Oxidizing Atmosphere.** *Oxidation of Metals* 2017; **87**(5–6): 717–727.

[20] ASTM C618-19. **Standard Specification for Coal Fly Ash and Raw or Calcined Natural Pozzolan for Use in Concrete.** ASTM International, West Conshohocken, PA; 2019.

[21] Bayat O. **Characterisation of Turkish Fly Ashes.** *Fuel* 1998; 77(9–10): 1059–1066.

[22] Al Ghouti MA, Ghrair A, Khoury H, Al-Degs YS, Khraisheh M. **Fly Ash Generated from Heavy Fuel Incineration in Power Plants: Physical and Chemical Characteristics.** *Indian Journal of Environmental Sciences* 2012; **7**(11): 829–838.

[23] Al-Degs YS, Ghrir A, Khoury H, Walker GM, Sunjuk M, Al-Ghouti MA. **Characterization and Utilization of Fly Ash of Heavy Fuel Oil Generated in Power Stations.** *Fuel Processing Technology* 2014; **123**: 41–46.

[24] Verma P, Kumar A, Chauhan SS, Verma M, Malik RS, Choudhary V. **Industrially Viable Technique for the Preparation of HDPE/Fly Ash Composites at High Loading: Thermal, Mechanical, and Rheological Interpretations.** *Journal of Applied Polymer Science* 2018; **135**(11): 459951.

[25] ASTM D792-20. **Standard Test Methods for Density and Specific Gravity (Relative Density) of Plastics by Displacement.** ASTM International, West Conshohocken, PA; 2020.

[26] Kaw AK. **Mechanics of Composite Materials.** 2nd ed. CRC Press, Boca Raton; 2005.

[27] Cao Z, Daly M, Geever LM, Major I, Higginbotham CL, Devine DM. **Synthesis and Characterization of High Density Polyethylene/Peat Ash Composites.** *Composites Part B: Engineering* 2016; **94**: 312–321.

[28] ASTM D2734-09. **Standard Test Methods for Void Content of Reinforced Plastics.** ASTM International, West Conshohocken, PA; 2009.

[29] ASTM D570-98. **Standard Test Method for Water Absorption of Plastics.** ASTM International, West Conshohocken, PA; 2018.

[30] Kord B, Roohani M. **Water Transport Kinetics and Thickness Swelling Behavior of Natural Fiber-Reinforced HDPE/CNT Nanocomposites.** *Composites Part B: Engineering* 2017; **126**: 94–99.

[31] ASTM D2240-05. **Standard Test Method for Rubber Property—Durometer Hardness.** ASTM International, West Conshohocken, PA; 2010.

[32] ASTM G99-17. **Standard Test Method for Wear Testing with a Pin-On-Disk Apparatus.** ASTM International, West Conshohocken, PA; 2017.

[33] Syduzzaman M, Akter M, Mahmud F, Bhowmick DR, Maliha AS, Fahmi FF, Jahan N, Alam MA. **Tensile Properties of Banana Fiber Reinforced Recycled High-Density Polyethylene Composites: An Experimental Investigation.** *SPE Polymers* 2024; **5**(3): 315–326.

[34] Savaş S, Gurbanov N, Doğan M. **Effect of Fiber Type, Fiber Content, and Compatibilizer on Two-Body Abrasive Wear Performance of HDPE Matrix Composites.** *Journal of*

Composite Materials 2019; **53**(19): 2743–2760.

[35] Jena KK, Alhassan SM. **Melt Processed Elemental Sulfur Reinforced Polyethylene Composites.** *Journal of Applied Polymer Science* 2016; **133**(9): 43060.

[36] Dhakal HN, Zhang Z. **Polymer Matrix Composites: Moisture Effects and Dimensional Stability.** *Wiley Encyclopedia of Composites*. Wiley; 2012. p. 1–7.

[37] Satapathy S. **Development of Value-Added Composites from Recycled High-Density Polyethylene, Jute Fiber and Flyash Cenospheres: Mechanical, Dynamic Mechanical and Thermal Properties.** *International Journal of Plastics Technology* 2018; **22**(2): 386–405.

[38] Satapathy S, Kothapalli RVS. **Influence of Fly Ash Cenospheres on Performance of Coir Fiber-Reinforced Recycled High-Density Polyethylene Biocomposites.** *Journal of Applied Polymer Science* 2015; **132**(28): 42211.

[39] Chand N, Sharma P, Fahim M. **Correlation of Mechanical and Tribological Properties of Organosilane Modified Cenosphere Filled High Density Polyethylene.** *Materials Science and Engineering: A* 2010; **527**(21–22): 5873–5878.

[40] Annaz AA, Irhayyim SS, Hamada ML, Hammood HS. **Comparative Study of Mechanical Performance between Al-Graphite and Cu-Graphite Self-Lubricating Composites Reinforced by Nano-Ag Particles.** *AIMS Materials Science* 2020; **7**(5): 534–547.

[41] Ramanjaneyulu S, Murthy BSN, Kumar SP, Gupta PSVNB. **Enhancing HDPE Properties: Impact of Nano-TiO2 and Nano-SiO2 Particles on Mechanical Properties and Wear Resistance.** *Journal of The Institution of Engineers (India): Series D* 2024; **105**(1): 245–256.

[42] Li K, Tjong SC. **Preparation and Mechanical and Tribological Properties of High-Density Polyethylene/Hydroxyapatite Nanocomposites.** *Journal of Macromolecular Science, Part B* 2011; **50**(7): 1325–1337.

[43] Yang D, He QC. **Micromechanical Estimation of the Effective Wear of Elastoplastic Fiber-Reinforced Composites.** *International Journal of Non-Linear Mechanics* 2019; **108**: 11–19.

[44] Sudheer M, Prabhu R, Raju K, Bhat T. **Modeling and Analysis for Wear Performance in Dry Sliding of Epoxy/Glass/PTW Composites Using Full Factorial Techniques.** *ISRN Tribology* 2013; **2013**: 1–11.

[45] Haiter Lenin A, Vettivel SC, Raja T, Belay L, Singh SCE. **A Statistical Prediction on Wear and Friction Behavior of ZrC Nano Particles Reinforced with Al Si Composites Using Full Factorial Design.** *Surfaces and Interfaces* 2018; **10**: 149–161.

[46] Gangatharan K, Selvakumar N. **Optimizing the Dry Sliding Wear Behavior of Copper Hybrid Nano Composites Reinforced with MWCNTs and Nano B4C Using Full Factorial Design.** *Transactions of the Indian Institute of Metals* 2016; **69**(3): 717–732.

[47] Bhushan B. **Introduction to Tribology.** 2nd ed. John Wiley & Sons, New York; 2013.